

Article

Icariin/Aspirin Composite Coating on TiO₂ Nanotubes Surface Induce Immunomodulatory Effect of Macrophage and Improve Osteoblast Activity

Aobo Ma [†], Yapeng You [†], Bo Chen, Wanmeng Wang, Jialin Liu, Hui Qi, Yunkai Liang, Ying Li ^{*} and Changyi Li ^{*}

School of Dentistry, Tianjin Medical University, Tianjin 300070, China; maaobo@tmu.edu.cn (A.M.); youyapeng@tmu.edu.cn (Y.Y.); chenbo@tmu.edu.cn (B.C.); wangwanmeng@tmu.edu.cn (W.W.); liujialin@tmu.edu.cn (J.L.); qihui@tmu.edu.cn (H.Q.); liangyunkai@tmu.edu.cn (Y.L.)

^{*} Correspondence: yingli@tmu.edu.cn (Y.L.); lichangyi@tmu.edu.cn (C.L.);

Tel.: +86-22-23332034 (Y.L.); +86-22-23332003 (C.L.)

[†] These authors contributed equally to this work.

Received: 24 March 2020; Accepted: 22 April 2020; Published: 24 April 2020



Abstract: Surface coating modification of titanium-based alloys is an efficient way to accelerate early osseointegration in dental implant fields. Icariin (ICA) is a traditional Chinese medicine that has bone activating functions, while aspirin (ASP) is a classical non-steroidal anti-inflammatory drug with good antipyretic and analgesic capabilities. Moreover, poly(lactic-co-glycolic acid) (PLGA) has attracted great attention due to its excellent biocompatibility and biodegradability. We superimposed an ASP/PLGA coating onto ICA loaded TiO₂ nanotubes structure so as to establish an icariin/aspirin composite coating on TiO₂ nanotubes surface. Scanning electron microscopy, X-ray photoelectron spectroscopy, a contact angle test and a drug release test confirmed the successful preparation of the NT-ICA-ASP/PLGA substrate, with a sustained release pattern of both ICA and ASP. Compared to those cultured on the Ti surface, macrophage cells on the NT-ICA-ASP/PLGA substrate displayed decreased M1 proinflammatory and enhanced M2 proregenerative genes and proteins expression, which implied activated immunomodulatory effect. Moreover, when cultured with conditioned medium from macrophages, osteoblast cells on the NT-ICA-ASP/PLGA substrate revealed improved cell proliferation, adhesion and osteogenic genes and proteins expression, compared with those on the Ti surface. The abovementioned results suggest that the established NT-ICA-ASP/PLGA substrate is a promising candidate for functionalized coating material in Ti implant surface modification.

Keywords: icariin; aspirin; composite coating; TiO₂ nanotubes; immunomodulatory effect; macrophage; osteoblast activity

1. Introduction

Dental implant dentures are the preferred treatment option for patients with dentition defect and edentulous jaws [1]. Titanium and titanium-based alloys have become the main steam material for dental implants due to their excellent mechanical properties and biocompatibility [2]. However, the biological inertness of pure titanium impairs the rapid bonding between dental implant and bone tissue, even causes implant failure [3]. Therefore, surface modification of Ti-based implant materials has become the main way to enhance cell activity, exert antibacterial effect and so as to promote osseointegration [4]. Various strategies have been employed for improving surface characteristics of dental implant, including physical, chemical and biological methods [5].

Among them, the application of protein growth factor on implant surface has been proved to be an effective way for enhancing osteogenesis and could accelerate osseointegration at the implant-tissue

interface, such as bone morphogenetic protein-2 [6–8]. However, the lack of chemical stability of growth factor proteins hinders their wide application in implant surface modification [8,9]. In addition, inflammation reaction generated during the drilling, screwing and inserting processes of implant surgery may hamper bonding strength between implant and surrounding bone tissue [10]. In order to overcome the drawbacks, it becomes imperative to develop a new surface modification method, which could load osteogenic drug with chemical stability and subside inflammation accompanied with implant surgery at the same time.

Epimedium is widely used in traditional Chinese medicine and has the kidney invigorating and bone activating functions [11]. Icariin (ICA), an inexpensive and chemically stable monomer components of Epimedium [12,13], retains the osteogenic function of Epimedium and has antiatherosclerotic, anti-inflammatory and anticancer capabilities [14]. At the same time, icariin can promote the proliferation activity of osteoblasts and inhibit the formation of osteoclasts. Therefore, it is widely used in the treatment of osteoporosis [15]. In addition, icariin is also a promising osteoinductive compound for bone tissue engineering [11,16]. We previously reported that the icariin-functionalized coating on TiO₂ nanotubes surface promote osteoblast function and accelerate osseointegration [17]. Moreover, recently the anti-inflammatory [18,19] and immunoregulatory [20] functions of ICA has also been raised. Therefore, ICA becomes an ideal candidate drug for Ti-based implant surface modification to regulate immune response and promote bone formation at the same time.

Aspirin (ASP) is a well-established non-steroidal anti-inflammatory drug (NSAID), with chemical stability and an inexpensive price. In addition to its long-term application as an antipyretic and analgesic for postoperative pain relief [21], ASP is also reported to substantially improve immunomodulatory function, manifested as regulatory T cells upregulation and Th17 cells downregulation in vitro [22]. In addition, systemic use of ASP revealed enhanced bone regeneration in vivo [23]. Moreover, some scholars have recently demonstrated that low doses of ASP can regulate the balance between bone resorption and bone formation in osteoporosis caused by ovariectomy [24–26]. Evidence from both in vitro cell culture tests and in vivo animal studies also revealed that ASP has a protective effect on bones by promoting the proliferation of osteoblast precursor cells and differentiation of osteoblasts [27]. Therefore, in the present work, we further superimposed ASP on the ICA-loaded TiO₂ nanotubes surface, in order to simultaneously resolve acute inflammation after implant insertion and improve osteogenesis.

Due to the lack of immobilization sites for drug molecules on the pristine Ti surface, we fabricated TiO₂ nanotubes on Ti surface as the reservoir for drug storage and delivery. Prepared by anodization, TiO₂ nanotubes are widely used as a surface modification method for dental implants [28]. It is well-accepted that nanostructured morphology can promote osteoblast adhesion, proliferation, differentiation activity and accelerate osseointegration around the implant [29]. However, since the end of nanotubes are in an open state, loading drug on TiO₂ nanotubes surface may cause undesired early burst release of the drug [30]. To solve this problem, it is necessary to find a coating material combined with nanotube architecture so as to endow the modified surface with a controlled drug release platform.

In order to effectively overcome the initial fast drug release of the simple TiO₂ nanotubes surface, various coatings were applied to acquire sustained drug release capacity on the nanotubes surface [31,32]. Among them, poly(lactic-co-glycolic acid), often shortened to PLGA, is one of the important materials for preparing controlled drug release coatings. A large amount of literature have reported different types of PLGA-based drug delivery systems (DDSs), such as nanoparticles, microspheres, implants, nanogels, nanofibers, rods, films, etc. [33,34]. The PLGA controlled release coating can load a variety of substances from hydrophilic to lipophilic drugs, from micromolecule to macromolecule and from single molecules to multiple molecules [35].

Therefore, in the present study, TiO₂ nanotubes structure were first prepared on the Ti surface and then loaded with ICA. Afterwards, the ASP/PLGA coating is employed to cover the pre-existed ICA loaded nanotubes surface. Thus, we constructed the icariin/aspirin composite coating on TiO₂

nanotubes surface, abbreviated as NT-ICA-ASP/PLGA substrate. Scanning electron microscope (SEM), X-ray photoelectron spectroscopy (XPS) and contact angle test were utilized for characterization of the physical and chemical features of the established icariin/aspirin composite coating on TiO₂ nanotubes surface. While the drug release tests were used to evaluate the release profiles of ICA and ASP, respectively.

Previously, researchers have made great effort on titanium surface modification to improve osteogenic properties in mesenchymal stem cells or osteoblast cells. However, the discrepancies of biological responses between in vitro and in vivo experiments exist when evaluating implant materials so far. It implies that the complexity of the in vivo environment has not been fully understood and some important factors, including immunomodulatory factors, are often ignored [36,37]. Among all the immune cells, macrophages play a central role in inflammation reaction [38,39]. Macrophage cells were also one of the cell types, which firstly contact with implant materials after insertion [40]. Therefore, in the present work, we intend to simultaneously explore the immunomodulatory function and osteogenic effect of the icariin/aspirin composite coating on TiO₂ nanotubes surface. At first, we examined the immunomodulatory effect of the established NT-ICA-ASP/PLGA substrate using macrophage cells. Then, we employed the indirect coculture system including macrophage conditioned media (CM) and osteoblast cells to evaluate the osteogenic function of the constructed NT-ICA-ASP/PLGA substrate.

Our hypothesis is that icariin/aspirin composite coating on the TiO₂ nanotubes surface could improve osteogenic effect of osteoblast cells through regulating the polarized status of macrophages. By exerting immunomodulatory function of macrophages at the interface between implant and surround bone tissue, an immune microenvironment that favors bone formation is created. The combined effects of icariin and aspirin may synergistically accelerate osseointegration of the dental implant.

2. Materials and Methods

2.1. Chemicals and Reagents

ICA and ASP was provided by Sigma-Aldrich (St. Louis, MO, USA). PLGA (Resomer RG 503, lactide:glycolide 50:50, ester terminated, Mw 24,000–38,000) was provided by Sigma-Aldrich. Phosphate buffered saline (PBS) was obtained from Solarbio, Inc. (Beijing, China). Ammonium fluoride (NH₄F) and ethylene glycol (EG) were provided by Tianjin FengChuan Chemical Reagent Co., Ltd (Tianjin, China).

2.2. Specimen Preparation and Surface Characterization

2.2.1. TiO₂ Nanotubes Fabrication

To prepare the TiO₂ nanotubes surface, titanium (Ti) discs with diameter of 15 mm and thickness of 1 mm were fabricated from commercially produced titanium plate (Grade 2, ASTM F67 unalloyed Ti; 99.7% Ti; 0.14% O; 0.09% Fe; 0.04% C; 0.02% N; 0.008% H; 0.002% other elements), which were purchased from Baoji Titanium Industry (Baoji, China). Ti discs were polished by 320, 800, 1500 and 2000 grit sand paper in sequence, ultrasonically washed with acetone, ethanol and deionized water in turn for 10 min, and then dried in air. The solvent of the electrolyte is ethylene glycol (EG), the solute is 0.16 mol/L NH₄F, with 10% deionized water by volume added. The TiO₂ nanotubes discs were fabricated under a voltage of 40 V for 1 h by high-voltage DC power supply (Dongwen High Voltage Power Supply Factory, Tianjin, China). After reaction, discs were ultrasonically cleaned by the EG solution. Later, the discs were rinsed with deionized water for 3 times, and left to dry naturally to obtain the TiO₂ nanotubes (NT) surface.

2.2.2. Construction of Icariin/Aspirin Composite Coating on the TiO₂ Nanotubes Surface

To fabricate the NT-ICA surface, ICA was dissolved in anhydrous methanol, with the concentration adjusted to 1.15 mg/mL, then the solution was mixed by vortex oscillators for 2 min. The NT slices were

placed in the wells of a 24-well plate, one well for each slice, then 1 mL prefabricated ICA solution was added to each well, sealed with parafilm membrane and left to stand for 24 h at 4 °C. After that, the excess liquid was sucked out and air-dried to obtain the NT-ICA surface.

To construct the Ti-PLGA and NT-ICA-PLGA surfaces, we dissolved 30 mg of PLGA powder in 1 mL acetone solution, mixed thoroughly by vortex. We spread 100 µL mixed solution evenly on the surface of the Ti and the NT-ICA slices, dried naturally and repeated four times to obtain the Ti-PLGA and NT-ICA-PLGA surfaces, respectively.

To establish the NT-ASP/PLGA and NT-ICA-ASP/PLGA substrates, we took 30 mg PLGA and 10 mg ASP powder into a 15 mL centrifuge tube, add 1 mL acetone solution, and mix thoroughly by vortex. Then apply 100 µL of the mixed solution of ASP, PLGA and acetone to the surface of the NT and NT-ICA slices and left to dry naturally. Repeat the coating step four times to obtain the NT-ASP/PLGA and NT-ICA-ASP/PLGA substrates, respectively.

2.2.3. Surface Characterization

Observe the macro surface morphology of Ti, Ti-PLGA, NT, NT-ICA, NT-ICA-PLGA, NT-ASP/PLGA and NT-ICA-ASP/PLGA surfaces with stereomicroscope (S9i; Leica Microsystem, Tokyo, Japan). The micro surface topography of various surfaces was observed using a scanning electron microscope (SEM, Zeiss Merlin Compact; ZEISS, Jena, Germany), the working distance was 22.4–27.8 mm. X-ray photoelectron spectroscopy (XPS, AXIS Nova; Kratos Analytical, Manchester, UK) was used for analyzing the elemental composition of each sample's constituents. At room temperature, the wettability of the sample surfaces were evaluated by contact angle measurement using deionized water. The droplet volume used was 2 µL, and a contact angle goniometer (JGW-360A, Chongda Intelligent Technology, Xiamen, China) was used to acquire droplet images. Values of initial contact angle were analyzed using image analysis software (version 1.0, Anglem, Chongda Intelligent Technology, Xiamen, China). Three different positions were measured for each sample, and values were determined as mean ± standard deviation, $n = 3$.

2.3. Icaritin and Aspirin Drug Release Amount Measurement

The drug release profiles of two drugs ICA and ASP were detected by the high performance liquid chromatography system (HPLC; 1100 Series; Agilent Technologies, Santa Clara, CA, USA). The MS 105 electronic balance (Mettler-Toledo, Greifensee, Zurich, Switzerland) of 0.01 mg accuracy was used to accurately weigh the ICA and ASP reference substance. Anhydrous methanol was used to prepare the standard solution used in the standard curve by half dilution method. The standard solution concentrations of ICA and ASP are 0, 0.5, 1, 2, 4, 8 and 16 µg/mL and 0, 2.5, 5, 10, 20, 40 and 80 µg/mL, respectively. The samples were immersed in PBS (pH 7.4) at 37 °C for drug release experiments. Various samples were immersed in 10 mL PBS and incubated for 24 h, and then the solution was daily collected for analysis by the HPLC system. After that, fresh PBS solution was added to replace the extracted solution. The test periods for ICA and ASP lasted for 30 and 8 days, respectively. The total amount of drug loaded on the sample was calculated according to the accumulated amount of drug released until the end of the test period used in this experiment. The drug cumulative release percentage was calculated by dividing the accumulated amount of released drug at each time point by the total amount of drug loaded. Data are collected from three separate experiments and expressed as mean ± SD ($n = 3$).

2.4. Behaviors of RAW 264.7 Cells Cultured on Different Surfaces

2.4.1. Cell Culture of Macrophage Cells

All samples were sterilized by irradiation with 25 kGy Cobalt 60 for 30 min and placed in 24-well plate. RAW 264.7 macrophage cells (American Type Culture Collection, ATCC, Manassas, VA, USA) were cultured in Dulbecco's modified eagle medium (DMEM, Gibco, Carlsbad, CA, USA) supplemented

with 10% fetal bovine serum (FBS, Gibco, Carlsbad, CA, USA) and 1% (*v/v*) streptomycin/penicillin (Gibco, Carlsbad, CA, USA) in a 5% CO₂ incubator (Thermo Fisher Scientific, Waltham, MA, USA) at 37 °C. Culture medium was daily changed and cells were stimulated with Lipopolysaccharides (LPS; Sigma Aldrich, St Louis, MO, USA) at the concentration of 1 µg/mL for the first three days. All samples were sterilized by irradiation with 25 kGy Cobalt 60 for 30 min.

2.4.2. Proinflammatory (M1) and Proregenerative (M2) Marker Gene Expression

The gene expression levels of proinflammatory (M1) and proregenerative (M2) markers in RAW 264.7 macrophage cells cultured on different substrates were analyzed by quantitative real-time polymerase chain reaction (qPCR). RAW 264.7 macrophage cells were seeded on all surfaces at a density of 1×10^4 cells/well for 3 days. Then, total RNA was extracted by TRIzol (Thermo Fisher Scientific, Waltham, MA, USA). The RNA concentration and purity were measured at 260 nm by Nanodrop spectrophotometer (NanoDrop Technologies, Wilmington, DE, USA). Mouse mRNA encoding genes for tumor necrosis factor-alpha (TNF- α), interleukin-1 β (IL-1 β), transforming growth factor-beta (TGF- β) and heme oxygenase-1 (HO-1) were selected, glyceraldehyde-3-phosphate dehydrogenase (GAPDH) was amplified in parallel with the target genes and used as an internal control. Reverse transcription and qPCR were performed. Then relative gene expression levels were determined using the relative threshold cycle (CT) method and reported as $2^{-\Delta\Delta C_t}$. Primers used for both the target genes and the housekeeping gene were shown in Table 1. For every interested gene, the cDNA amplification was performed in triplicate by a single sample. The results were from three independent tests.

Table 1. Primers for proinflammatory (M1) and proregenerative (M2) marker genes.

Gene	Gene Bank ID	DNA Primer	Sequence	Size (bp)
TNF- α	NM_001278601.1	Forward	5'-TGCCTAIGTCTCAGCCTCTTC-3'	117
		Reverse	5'-GAGGCCATTTGGGAACCTTCT-3'	
IL-1 β	NM_008361.4	Forward	5'-TGTGCAAGTGTCTGAAGCAGC-3'	129
		Reverse	5'-TGGAAGCAGCCCTTCATCTT-3'	
TGF- β	NM_011577.2	Forward	5'-TTGCTTCAGCTCCACAGAGA-3'	183
		Reverse	5'-TGGTTGTAGAGGGCAAGGAC-3'	
HO-1	NM_010442.2	Forward	5'-GCCGAGAATGCTGAGTTCATG-3'	86
		Reverse	5'-TGGTACAAGGAAGCCATCACC-3'	
GAPDH	NM_008084.3	Forward	5'-GGTGAAGGTCGGTGTGAACG-3'	233
		Reverse	5'-CTCGCTCCTGGAAGATGGTG-3'	

2.4.3. Enzyme-Linked Immunosorbent (ELISA) Assay

The proinflammatory (M1) and proregenerative (M2) marker protein expression levels in RAW 264.7 macrophage cells incubated with all kinds of samples were further measured by enzyme-linked immunosorbent (ELISA) assay. RAW 264.7 macrophage cells were seeded on different surfaces at a density of 1×10^4 cells/well for 3 days. The supernatants were then collected and measured immediately. The concentrations of proteins including tumor necrosis factor-alpha (TNF- α), interleukin-1 β (IL-1 β), transforming growth factor-beta (TGF- β) and heme oxygenase-1 (HO-1) were determined by ELISA kits (ImmunoWay Biotechnology, Plano, TX, USA). Three different slices were measured for each group. Three independent experiments were repeated.

2.5. Behaviors of MC3T3-E1 Cells on Various Surfaces in Conditioned Medium (CM)

2.5.1. Collection and Preparation of CM

RAW 264.7 macrophages were seeded on various surfaces at a density of 1×10^4 cells/well for 14 days. Cells were stimulated with LPS (1 µg/mL) for the first three days, and culture medium supernatant were collected daily and changed with new medium. The collected supernatant was centrifuged at 1500 rpm for 15 min, and then filtered through a 0.22 µm filter. Then, the filtered

supernatant was mixed with DMEM containing 10% FBS and 1% penicillin/streptomycin at a volume ratio of 1:1 to obtain the conditioned medium (CM), and stored at 4 °C for later use.

2.5.2. Cell Culture of Osteoblast Cells

MC3T3-E1 preosteoblast cells (ATCC, Manassas, VA, USA) were first cultured in the DMEM supplemented with 10% FBS and 1% (*v/v*) streptomycin/penicillin in a 5% CO₂ incubator at 37 °C. After 4 h of inoculation, cells were seeded on different surfaces at a density of 1×10^4 cells/well and the CM prepared in 2.5.1 was used for cell culture. Various samples were disinfected through irradiation with 25 kGy Cobalt 60 for 30 min.

2.5.3. Cell Proliferation

The cell proliferation ability of RAW 264.7 macrophage cells incubated with various substrates were measured using cell counting kit-8 assay (CCK-8, New Cell and Molecular Biotech, Suzhou, Zhejiang, China). Cells were cultured with all kinds of substrates in 24-well plates at a density of 1×10^4 cells/well for 7 days. At 1, 3, 5 and 7 d, 1 mL of culture medium containing 100 µL CCK-8 solution was distributed to each well. After incubation for 2 h in the incubator, 100 µL reserved solution was transferred into a new 96-well plate, and then measured by a microplate reader (Cytation 5, Bio-Tek, Winooski, VT, USA) at 450 nm. The values were measured and recorded as mean \pm standard deviation, $n = 3$. The cell proliferation tests were repeated three times.

2.5.4. Cell Morphology

To examine cell morphology on various surfaces, MC3T3-E1 cells were incubated with different surfaces for 24 h before observation. Then, all samples were rinsed twice with PBS, fixed with 2.5% glutaraldehyde solution (Solarbio, Beijing, China) at 4 °C overnight. Then the fixed cells were rinsed by PBS for three times, 10 min each time. Afterwards, samples were further fixed by 1% osmic acid away from light for 1 h and then dehydrated using sequential ethanol solutions (30%, 50%, 75%, 90%, 95% and 100% (*v/v*)). Subsequently, various substrates were dried by critical point dryer (EM CPD030, Leica Microsystems, Wetzlar, Germany, the working distance was 8.3–9.4 mm. Lastly, cells grown on various samples were observed by SEM (SU8010, Hitachi, Tokyo, Japan). The typical images from three independent slices were shown for each group.

2.5.5. Osteogenic-Related Gene Expression

To detect the osteogenic-related gene expression levels in MC3T3-E1 cells incubated with different substrates, MC3T3-E1 cells were cultured for 14 days and the culture medium was changed daily. At 14 d, cells on the samples were extracted by TRIzol. Expression levels of mouse mRNA encoding genes for alkaline phosphatase (ALP), collagen type 1 alpha 1 (COL1A1), osteopontin (OPN) and osteocalcin (OCN) were detected, with the housekeeping gene *GAPDH* used as the internal control. Reverse transcription and quantitative real-time polymerase chain reaction were performed and data were calculated by the $2^{-\Delta\Delta C_t}$ method. Primers used for the target genes and the housekeeping genes were shown in Table 2. The cDNA amplification of each gene of interest was conducted in triplicate by one sample and data were reported from three separate tests.

Table 2. Primers for osteogenesis-related genes.

Gene	Gene Bank ID	DNA Primer	Sequence	Size (bp)
ALP	NM_007431.3	Forward	5'-ATCTTTGGTCTGGCTCCCATG-3'	106
		Reverse	5'-TTTCCCGTTCACCGTCCAC-3'	
COL1A1	NM_007742.4	Forward	5'-TAAGGGTCCCAATGGTGAGA-3'	203
		Reverse	5'-GGGTCCCTCGACTCCTACAT-3'	
OPN	NM_001204203.1	Forward	5'-CTCACATGAAGAGCGGTGAG-3'	174
		Reverse	5'-TCTCCTGGCTCTCTTTGGAA-3'	
OCN	NM_007541.3	Forward	5'-GGACCATCTTTCTGCTCACTCTG-3'	131
		Reverse	5'-GTTCACTACCTTATTGCCCTCCTG-3'	
GAPDH	NM_008084.3	Forward	5'-GGTGAAGGTCCGTGTGAACG-3'	233
		Reverse	5'-CTCGCTCTGGAAGATGGTG-3'	

2.5.6. Western Blot Test

The osteogenic-related protein expression levels in MC3T3–E1 cells cultured with various surfaces were examined by Western blot test after 14 days of incubation. MC3T3–E1 cells were cultured for 14 days and medium changed daily. Cells were then harvested on ice, washed twice using PBS, and 200 μ L lysis buffer supplemented with protease inhibitor were added to each well. After being incubated on ice for 10 min, cell extracts were subjected to centrifuge with 12,000 rpm at 4 °C for 15 min. Protein samples were separated by SDS-PAGE and then transferred to polyvinylidene fluoride (PVDF) membranes. After blocking using skim milk powder (5 g/100mL, Solarbio, Beijing, China) for 1 h, PVDF membranes were hybridized with specific antibodies of ALP (1:1000, ab229126), COL1A1 (1:1000, ab6308), OPN (1:1000, ab63856) and OCN (1:1000, ab93876) from Abcam, Cambridge, UK, respectively overnight at 4 °C. Data of expression levels from interested proteins were compared with that of internal control beta-Actin (1:1000, ab8226, Abcam, Cambridge, UK) to normalize loaded protein amount of different samples. The membranes were washed three times, and then incubated with goat anti-mouse secondary antibody at 1:5,000 dilution for 1 h. The protein bands were visualized using chemiluminescence imaging system (ChemiDocTM XRS+ workstation, Hercules, CA, USA). The relative intensity of the protein bands was quantified using image analysis software (Image Pro-Plus 6.0, Media Cybernetics, Silver Spring, MD, USA).

2.6. Statistical Analysis

All experiments were performed three times and the data were expressed as means \pm standard deviations (SD). The one-way ANOVA combined with Tukey post hoc test was applied to examine the statistical difference between different samples. All differences considered to be significant when $p < 0.05$.

3. Results

3.1. Surface Characterization

First, the macro surface morphology of various surfaces was observed with stereomicroscope (S9i; Leica Microsystem, Tokyo, Japan) and shown in Figure 1. The Ti slice looks silver and the Ti-PLGA surface observed a transparent film covering the original Ti surface, suggesting that PLGA can form thin film materials on the prepared surface. For the NT surface, a faint gray-green color was seen after anodic oxidation. Whereas, the surface of NT-ICA samples had obvious yellow color, with scattered icariin particles deposited. The NT-ICA-PLGA surface obtained by dripping the PLGA solution on the surface of the NT-ICA sample was still yellow, but the original ICA particles were covered and difficult to identify. Since ASP and PLGA are both white, the NT-ASP/PLGA surface revealed a white-color film on the faint gray-green color NT base material. While for the NT-ICA-ASP/PLGA substrate, a white-color film covering yellow base of NT-ICA was seen.



Figure 1. Macro surface morphology of various surfaces was observed under stereomicroscope (S9i; Leica Microsystems, Tokyo, Japan) and representative images were shown (10 ×).

Second, the micro surface morphology of all samples was observed using a scanning electron microscope (SEM, Zeiss Merlin Compact; ZEISS, Jena, Germany). As shown in Figure 2, scratch marks were seen on the surface of Ti after gradient polishing. After loading the PLGA coating, the Ti-PLGA group displayed a smooth and uniform surface. After the anodizing process, nanotubes with uniform and controllable diameter and length can be detected on the surface of NT group. The diameter of nanotubes was 100 ± 5 nm, while the length of which was 3 ± 0.5 μm . On the surface of the NT-ICA group, scattered granular substances of ICA were observed. For the NT-ICA-PLGA surface, ICA was completely enwrapped by the uniform smooth film of PLGA coating, with many needle-like configurations indicating the existence of ICA. While on the NT-ASP/PLGA substrate, short needle-like ASP crystals were observed in the PLGA coating layer. The morphology of NT-ICA-ASP/PLGA surface combined the common features of NT-ASP/PLGA and NT-ICA-PLGA surfaces, and displayed both the configuration of ICA and ASP in the PLGA coating.

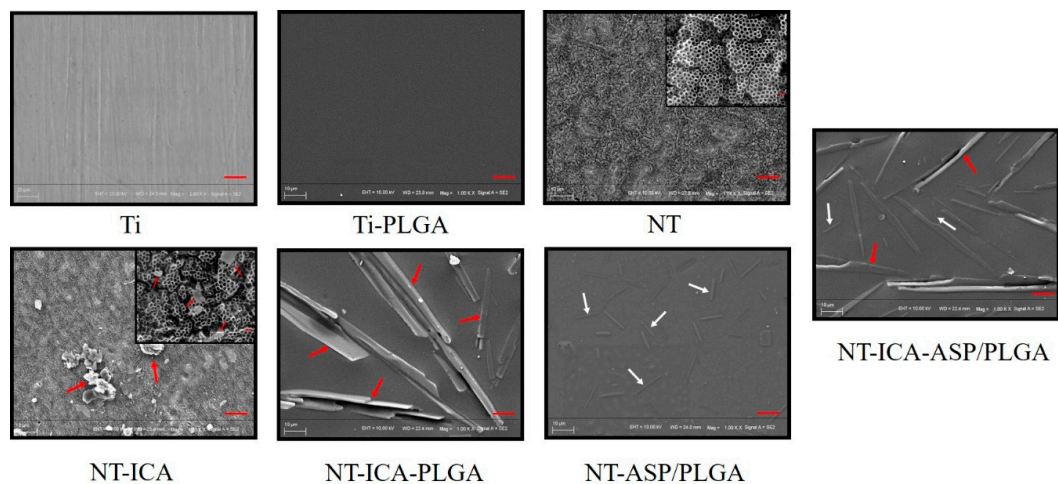


Figure 2. Surface micromorphology images of different substrates were obtained with scanning electron microscope (SEM, Zeiss Merlin Compact; ZEISS, Jena, Germany). Red and white arrows indicate icariin (ICA) and aspirin (ASP), respectively; 1000×, scale bar = 10 μm . Insets of images of NT and NT-ICA substrates were magnified SEM graphs (30,000×, scale bar = 200 nm).

XPS results were used to determine the elemental composition of different samples. All binding energies were referenced to the C 1s spectrum peak (284.8 eV) as an internal reference after calibrating peak position. As shown in Figure 3 and Table 3, the spectra of the Ti and NT mainly include C1s, O1s and Ti2p3. For the NT-ICA surface, increased peak of C1s may originate from ICA ($\text{C}_{33}\text{H}_{40}\text{O}_{15}$), while the decreased peak of Ti2p3 may be explained by the partial coverage of the TiO_2 nanotubes structure by ICA, compared to the NT surface.

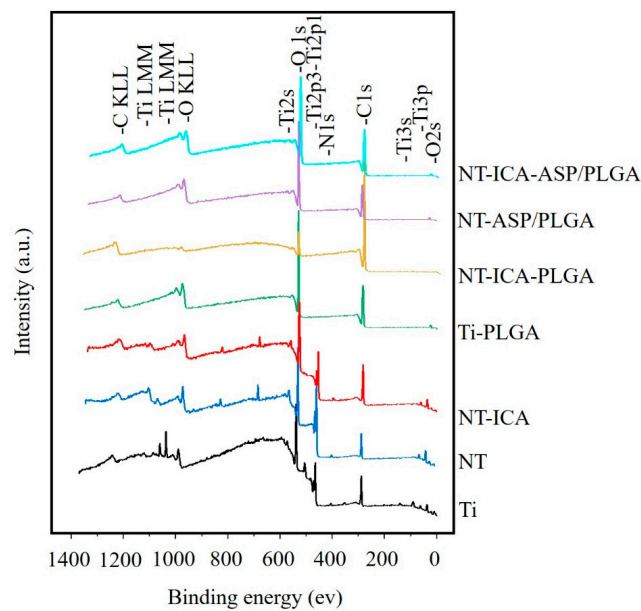


Figure 3. X-ray photoelectron spectroscopy (XPS) analysis displaying chemical composition of different surfaces.

Table 3. Chemical compositions of samples measured by XPS.

Substrates	C%	N%	O%	Ti%
Ti	47.19 ± 0.05	3.57 ± 0.01	39.27 ± 0.05	9.97 ± 0.02
Ti-PLGA	61.17 ± 0.05	0.34 ± 0.01	38.49 ± 0.03	0
NT	38.2 ± 0.03	2.97 ± 0.01	43.19 ± 0.03	15.63 ± 0.02
NT-ICA	50.49 ± 0.03	2.16 ± 0.01	39.47 ± 0.02	7.87 ± 0.02
NT-ICA-PLGA	90.66 ± 0.05	0	9.34 ± 0.02	0
NT-ASP/PLGA	72.3 ± 0.05	0	27.71 ± 0.02	0
NT-ICA-ASP/PLGA	64.53 ± 0.01	0	35.47 ± 0.05	0

In addition, the disappearance of the Ti peak on the Ti-PLGA, NT-ICA-PLGA, NT-ASP/PLGA and NT-ICA-ASP/PLGA surfaces indicate that the PLGA coating totally overspread the original Ti and nanotubes structures. As we known, PLGA $[(C_5H_8O_5)_n]$, ICA $(C_{33}H_{40}O_{15})$ and ASP $(C_9H_8O_4)$ are all composed of C, H and O. Due to the small photoionization cross section of H, the signal of H is too weak for XPS to be detected. Therefore, only C and O could be detected on the Ti-PLGA, NT-ICA-PLGA, NT-ASP/PLGA and NT-ICA-ASP/PLGA surfaces by XPS analysis. Moreover, since both icariin and aspirin have higher C and lower O element content than PLGA, the increased C and decreased O element content observed in NT-ICA-PLGA, NT-ASP/PLGA and NT-ICA-ASP/PLGA groups compared to the Ti-PLGA group may be explained by the successful loading of ICA and ASP.

In addition to surface topography and chemical composition, hydrophilicity is also an essential factor, which affects the biological compatibility of materials. Figure 4 showed that the contact angle of Ti was $89.5 \pm 0.6^\circ$, while after the application of PLGA coating, the contact angles decreased to Ti-PLGA ($69.5 \pm 0.6^\circ$), NT-ICA-PLGA ($58.9 \pm 0.8^\circ$), NT-ASP/PLGA ($69.8 \pm 0.5^\circ$) and NT-ICA-ASP/PLGA ($64.5 \pm 1.6^\circ$), respectively, with statistical significance. This indicates that PLGA coating could improve the wettability of surfaces, compared to pure Ti surface. Moreover, the contact angles of the NT and NT-ICA groups were $19.5 \pm 3.0^\circ$ and $21.3 \pm 1.0^\circ$, respectively, even lower than those of various PLGA coated substrates, with statistical significance. This phenomenon suggested that the titanium nanotube structure fabricated after anodization could substantially enhance the hydrophilicity of surfaces. In this experiment, we only detected the initial contact angles. In a follow-up experiment, we will further test the frequency acquisition of the droplet images and monitor the time dependence of the water

contact angle so as to obtain more kinetic constant and exponential parameters of material and evaluate hydrophilicity of the material much more accurately.

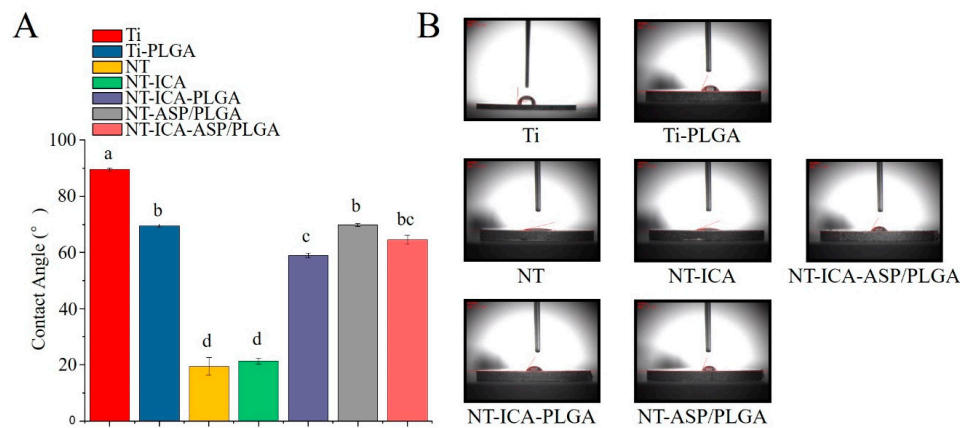


Figure 4. Contact angles of various surfaces. (A) Contact angle degree of different surfaces. Different lowercase letters indicate statistically significant differences between different groups ($p < 0.05$). Data are expressed as mean \pm SD, $n = 3$ replicates each group. (B) Images of contact angles on different surfaces.

3.2. In Vitro Drug Release Profile

The drug release pattern of ICA in the NT-ICA-ASP/PLGA surface is shown in Figure 5A. A sustained release profile of ICA was seen during the 30 days detection period. At the same time, the daily concentration of ICA always maintained within the range of $0.1\text{--}1 \times 10^{-5}$ mol/L per day, which was proved to be effective concentration of icariin to promote MC3T3-E1 cells osteogenesis in our preliminary experiment (data not shown). Taken into consideration of this point, the addition of ICA in the NT-ICA-ASP/PLGA surface is expected to exert continued osteogenic function during the release period.

As shown in Figure 5B, the release profile of ASP also displayed controlled release pattern during the release period, and finally reached a plateau at day 7. In addition, the release concentration of ASP maintained between 0.2 and 4 mM during day 1–5, within the effective concentration of anti-inflammatory and proregenerative function of ASP by our preliminary data (data not shown). Therefore, we hypothesized that the addition of ASP in the coating may promote RAW 264.7 macrophage cells to change from M1 to M2 polarization status.

Meanwhile, the release kinetics of both ICA and ASP in the NT-ICA-ASP/PLGA surface were assessed by fitting the release profiles of the two drugs to the Korsmeyer–Peppas model [41]. The mechanism of ICA and ASP release from the established surface during dissolution investigations in PBS was determined using Equation (1):

$$\frac{M_t}{M_\infty} = kt^n \quad (1)$$

where $\frac{M_t}{M_\infty}$ is the fractional drug release at denoted time point t , k is a kinetic constant reflecting the structural and geometric properties of the drug/carrier system, and n is the release exponent, which relies on the release mechanism. As shown in Figure 6, the first 10 days of ICA release profile was used for simulation and the release exponent n was 1 ± 0.0251 , which is close to a desirable time-dependent release mechanism, as indicated by Korsmeyer et al. [41]. While for ASP, since there were relatively less time points for simulation, we selected the first 4 days for simulation and the diffusional release exponent n value was 0.5438 ± 0.0725 , which implied a drug release mechanism approximately controlled by anomalous (non-Fickian) diffusion. As illustrated in Figure 6, the data fit the model well as the correlation coefficient R^2 of ICA and ASP release curves are 0.9946 and 0.9485, respectively. In addition, the kinetic constant of ICA and ASP were 5.9699 ± 0.2496 and 47.5629 ± 3.2833 ,

respectively, which indicated different structural and geometric properties of the two kinds of drugs in the drug/carrier system. The drug release percentage scatter diagrams as a function of time and sketch view of the established substrate were shown in Figure 6A–C. The sustained release mechanism of ICA may partly be interpreted by its poor water solubility [42] and the existence of the outside ASP/PLGA coating, which generate a viscous layer that further retarded the drug diffusion to the solvent, similar to a previous report [43]. In the future, drug release amount at more time points, especially for ASP, are needed to be measured to evaluate the kinetic mechanism much accurately.

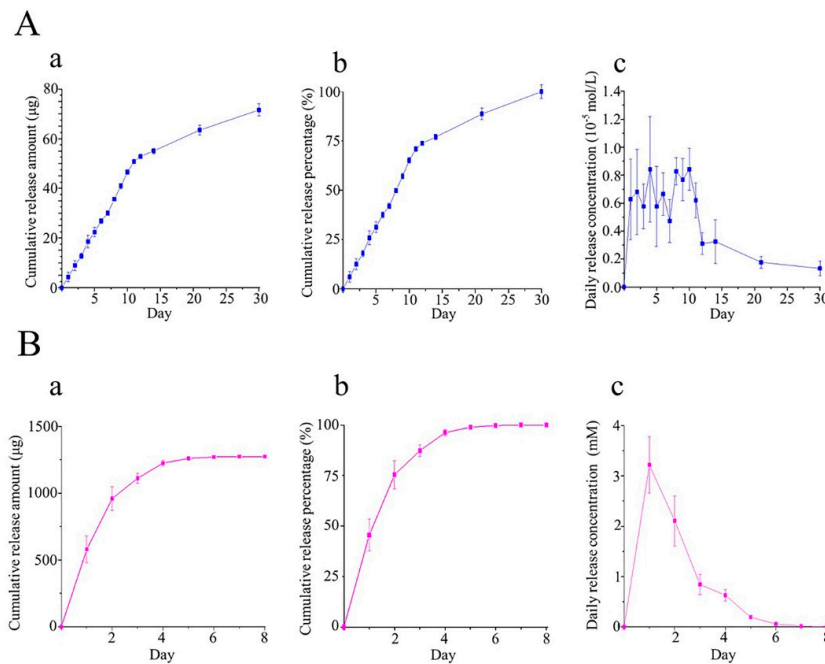


Figure 5. In vitro release profile of ICA (A) and ASP (B) on the NT-ICA-ASP/PLGA surface. (a) Cumulative release amount curve. (b) Cumulative release percentage curve. (c) Daily release concentration curve. Data are expressed as mean ± SD ($n = 3$).

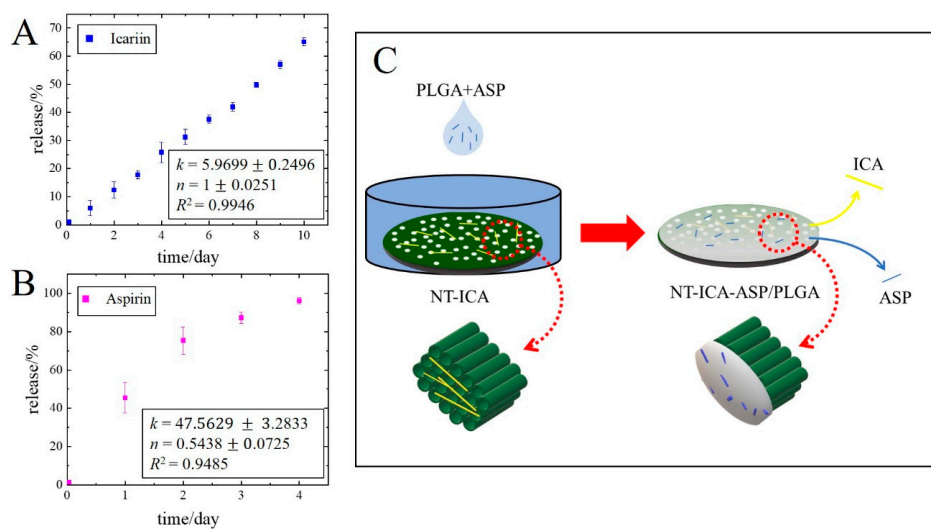


Figure 6. (A) ICA release behaviors in the first ten days. (B) ASP release behaviors in the first four days. (C) Sketch view of the NT-ICA-ASP/PLGA release system.

3.3. Polarization Status of RAW 264.7 Cells Cultured on Different Surfaces

3.3.1. Proinflammatory (M1) and Proregenerative (M2) Marker Genes Expression

Quantitative real-time polymerase chain reaction (qPCR) was performed to detect expression levels of proinflammatory (M1) and proregenerative (M2) gene markers in RAW 264.7 macrophage cells incubated with different substrates. The results were displayed in Figure 7. In the physiological healing of wound, the inflammatory phase last hours to days. Therefore, the initial several days after dental implant insertion was crucial for ideal osseointegration. Since the drug release curve of ASP revealed a relative steady release profile during day 2–4, we selected day 3 to evaluate the polarization of macrophages. As shown in Figure 7, M1 proinflammatory genes IL-1 β and TNF- α expression levels decreased in cells cultured on the NT surface, compared with those on the pristine Ti surface, indicating that the 100 nm diameter NT used in this experiment could inhibit inflammatory reaction at the gene level. Whereas the Ti-PLGA surface evoked higher proinflammatory genes expression than Ti surface. It indicated that although PLGA is a non-toxic and harmless material that can be absorbed by the human body, it could promote inflammatory reaction in RAW 264.7 cells during the early period after implantation. However, the decreased M1 proinflammatory gene levels in cells incubated with the NT-ICA-PLGA surface, compared with those with the Ti-PLGA surface implied that ICA may exert anti-inflammatory function. In particular, the addition of ASP, a well-established non-steroidal anti-inflammatory drug, obviously decreased proinflammatory gene expression in macrophage cells cultured on NT-ASP/PLGA and NT-ICA-ASP/PLGA substrates, compared with the Ti surface.

The M2 proregenerative marker genes expression in RAW 264.7 macrophage cells cultured on various surfaces were further evaluated. After 3 days of incubation, the addition of PLGA coating on the Ti-PLGA surface did not change TGF- β and HO-1 gene expression levels much, compared with Ti surface. It indicated that PLGA had no significant effect on induction of macrophages towards M2 polarized status. Previously, ICA has been reported to exert anti-inflammatory effect by elevated cytoprotective gene expression HO-1 [44,45]. Therefore, the observed highest HO-1 gene level on the NT-ICA surface may be attributed to the burst release of ICA occurred during the first 3 days, which evoked the substantially increased HO-1 gene expression. Most importantly, TGF- β and HO-1 gene levels in cells on the NT-ICA, NT-ICA-PLGA, NT-ASP/PLGA and NT-ICA-ASP/PLGA substrates were obviously higher than those on the Ti surface, with statistical significance. These results suggest that both ICA and ASP could induce M2 polarization of macrophage, which endowed the NT-ICA-ASP/PLGA substrate with superior proregenerative immunomodulatory ability.

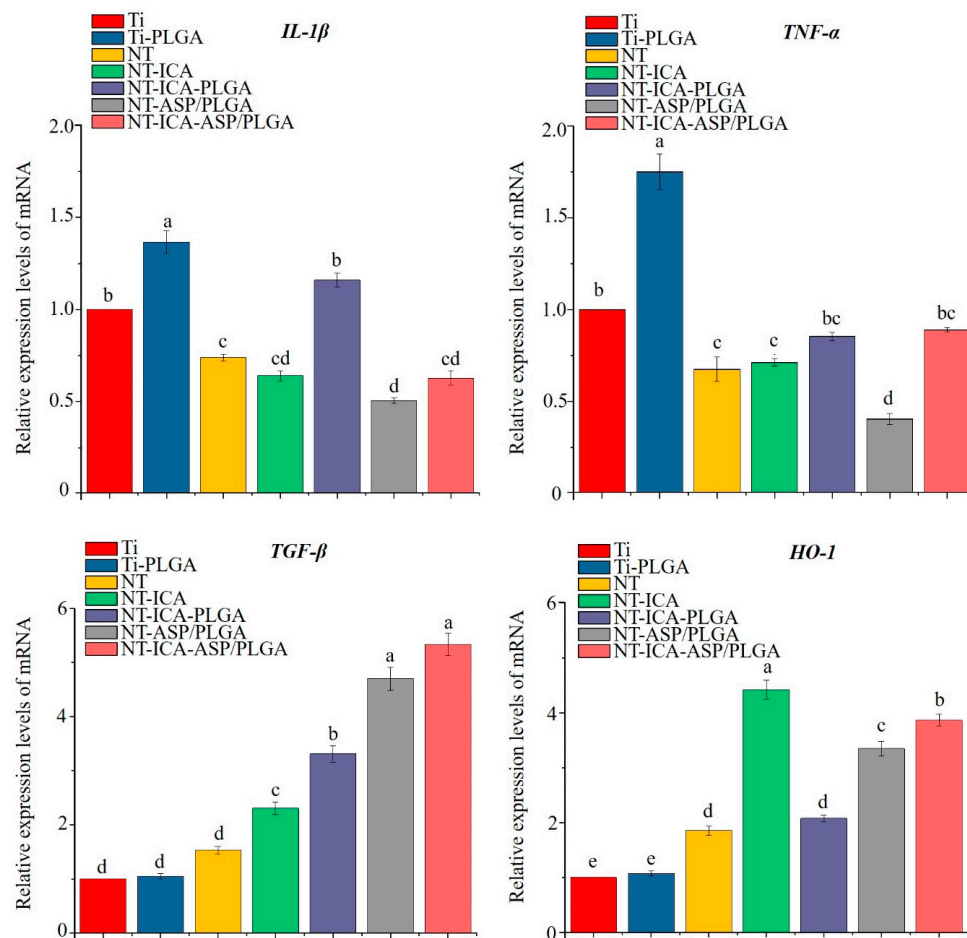


Figure 7. Real-time PCR results of interleukin-1 β (IL-1 β), tumor necrosis factor-alpha (TNF- α), transforming growth factor-beta (TGF- β) and heme oxygenase-1 (HO-1) gene expression levels in the RAW 264.7 cells on different substrates after 3 days of incubation. Different lowercase letters indicate statistically significant differences between different groups ($p < 0.05$). Data are mean \pm SD, $n = 3$ replicates each group.

3.3.2. Enzyme-Linked Immunosorbent (ELISA) Assay

We further examined the proinflammatory (M1) and proregenerative (M2) marker protein expression levels by ELISA assay. As shown in Figure 8, decreased IL-1 β and TNF- α and increased TGF- β and HO-1 protein levels were observed in cells cultured on the NT surface, compared with those on the Ti surface, displaying that the nanotube structure could reduce inflammation and induce regeneration. On the contrary, proinflammatory IL-1 β and TNF- α protein levels were enhanced, while the proregenerative TGF- β and HO-1 protein levels do not change much in cells on the Ti-PLGA surface, compared with the Ti surface. It showed that the PLGA coating could induce M1 inflammatory reaction, but failed to induce M2 polarization in macrophages. After the addition of ICA and ASP, M1 proinflammatory IL-1 β and TNF- α protein levels reduced, whereas TGF- β and HO-1 protein levels elevated in cells on the NT-ICA, NT-ICA-PLGA, NT-ASP/PLGA and NT-ICA-ASP/PLGA substrates, compared to the original Ti surface, with statistical significance. In particular, NT-ASP/PLGA and NT-ICA-ASP/PLGA groups had relatively lower M1 and higher M2 proteins secretion than the other groups.

Combined the results from gene and protein detection in RAW 264.7 cells, similar to the NT-ASP/PLGA surface, the NT-ICA-ASP/PLGA substrate also exhibited a superior ability of inflammation inhibition and regeneration enhancement than other surfaces. It implies that the

combination of ASP and ICA on the NT–ICA–ASP/PLGA surface could achieve anti-inflammatory and proregenerative function.

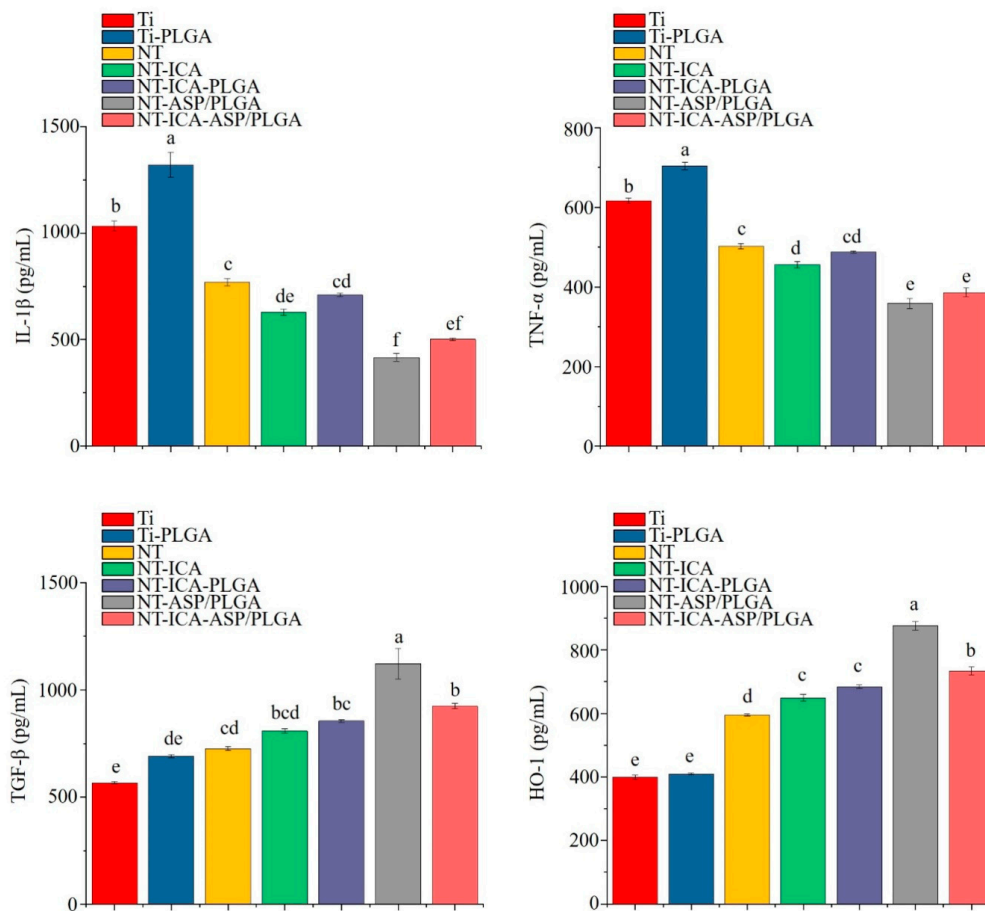


Figure 8. ELISA results representing the RAW 264.7 cytokine secretion on different substrates after 3 days of culture. Different lowercase letters indicate statistically significant differences between different groups ($p < 0.05$). Data are mean \pm SD, $n = 3$ replicates each group.

3.4. Behaviors of MC3T3-E1 Cells on Various Surfaces in Conditioned Medium (CM)

3.4.1. Cell Proliferation

The proliferation of MC3T3-E1 cells seeded on all samples was assessed by CCK-8 assay. Figure 9 showed cell numbers cultured on different surfaces after 1, 3, 5 and 7 days of incubation. At day 1 and 3, there was no statistical significance in the cell proliferation capacity of each group although a tendency of a higher cell proliferation rate on the NT–ICA–ASP/PLGA substrate was seen, compared with the Ti group. After 5 and 7 days of incubation, cells cultured on NT–ASP/PLGA and NT–ICA–ASP/PLGA substrates revealed higher cell proliferation ability compared with that on the pristine Ti, $p < 0.05$. This suggests the relative strong effect of aspirin to promote osteoblast proliferation under the existence of CM from macrophage cells. Interestingly, the proliferation rate of cells on the NT–ASP/PLGA group was moderately higher than that on the NT–ICA–ASP/PLGA group, although there was no statistical difference. This phenomenon may be explained by that the NT–ICA–ASP/PLGA substrate had an additional prodifferentiation effect on osteoblasts than the NT–ASP/PLGA surface, due to the existence of ICA. It is well accepted that during cell life activity, higher proliferation activity is often inhibited when cell differentiation is promoted and vice versa [12,46]. Therefore, the slightly inhibited cell proliferation of the NT–ICA–ASP/PLGA group may imply its enhanced cell differentiation due to the additional prodifferentiation effect of released ICA, compared to the NT–ASP/PLGA group.

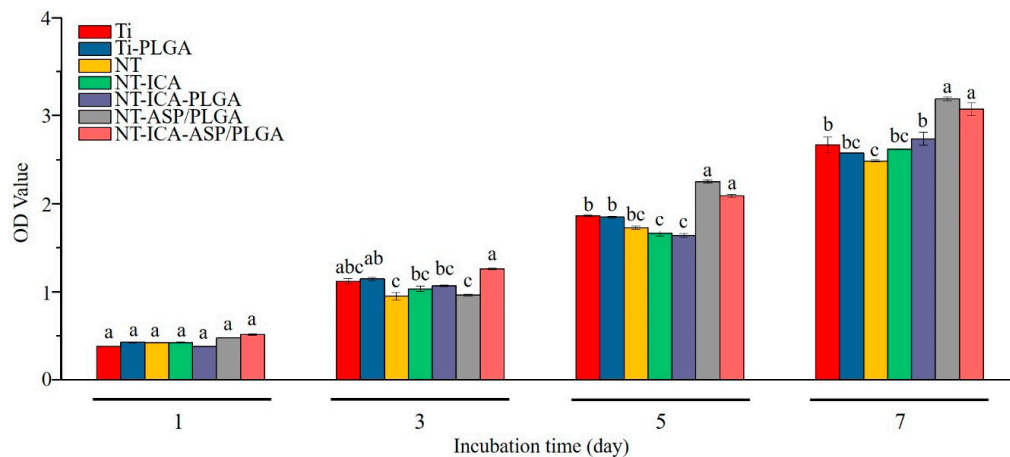


Figure 9. The CCK-8 results of MC3T3–E1 cells cultured on different surfaces for 1, 3, 5 and 7 days. Different lowercase letters indicate statistically significant differences between different groups ($p < 0.05$). Data are mean \pm SD, $n = 3$ replicates each group.

3.4.2. Cell Morphology

Cell morphologies of MC3T3–E1 osteoblast cells on different samples after 24 h of incubation were acquired with scanning electron microscope (SEM, SU8010, Hitachi, Tokyo, Japan) and shown in Figure 10. After 24 h of incubation, cells attached along the direction of scratch marks on the pure Ti surface. While on the NT and NT–ICA substrates, cells revealed well-distributed morphology, with filopodia stretching into the nanotubular structures, which implies good cell adhesion induced by the nanostructure. In addition, cells on the Ti–PLGA, NT–ICA–PLGA, NT–ASP/PLGA and NT–ICA–ASP/PLGA substrates displayed a spread-out morphology, towards different directions. This can be explained by that PLGA improved cell adhesion to some extent, similar with previous report [47]. In particular, for the NT–ICA–ASP/PLGA substrate, cells extend towards all directions, which revealed the satisfied cell adhesion ability.

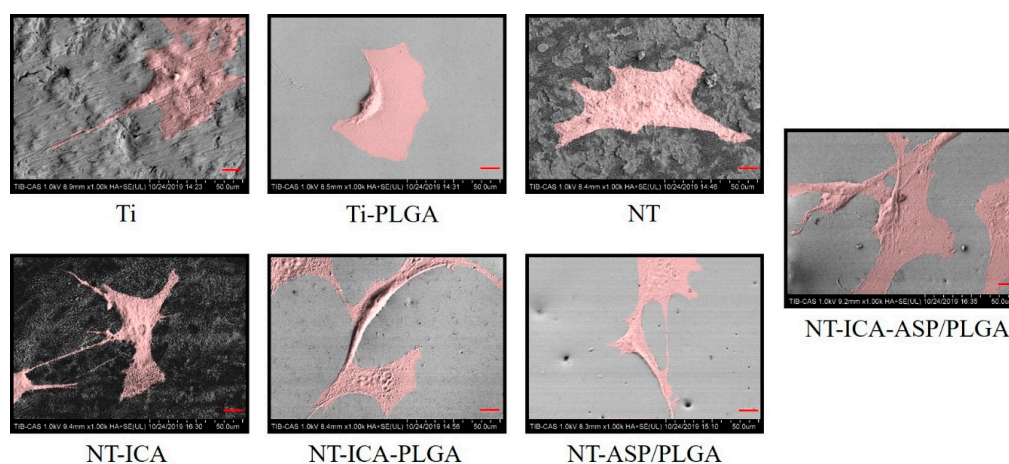


Figure 10. Images of MC3T3–E1 cells showing the representative morphology on different substrates after 24 h of culture were obtained with scanning electron microscope (SEM, SU8010, Hitachi, Tokyo, Japan). The pseudo colored pink cells indicate morphology of MC3T3–E1 cells; 1000 \times , scale bar = 10 μ m.

3.4.3. Osteogenesis-Related Gene Expression

Figure 11 shows osteogenesis-related genes expression of MC3T3–E1 cells cultured on different surfaces after 14 days of culture under the condition of macrophage CM. Gene expression levels of ALP, COL1A1 and OCN all increased on osteoblast cells cultured on the NT–ICA–PLGA, NT–ASP/PLGA and NT–ICA–ASP/PLGA substrates, compared with that on the pristine Ti and Ti-PLGA surfaces,

$p < 0.05$. It's worth noting that the NT-ICA-ASP/PLGA substrate showed highest expression levels for all of the osteogenesis-related genes examined than the other surfaces, with statistical significance. These results suggested that the employment of ICA and ASP could both improve osteoblast differentiation, and the superior osteogenic function of the NT-ICA-ASP/PLGA substrate lies in the synergistic function of ICA and ASP.

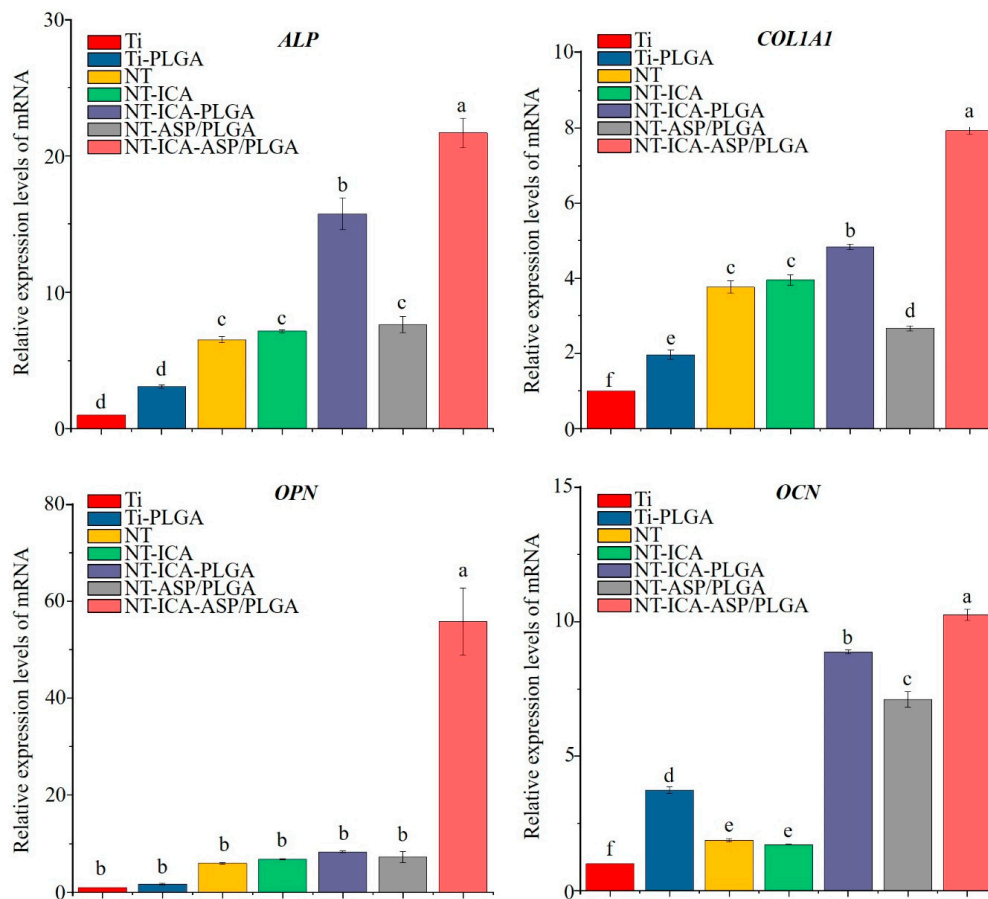


Figure 11. Real-time PCR results representing the gene expression levels of alkaline phosphatase (ALP), collagen type 1 alpha 1 (COL1A1), osteopontin (OPN) and osteocalcin (OCN) in MC3T3-E1 cells after 14 days of culture on different samples. Different lowercase letters indicate statistically significant differences between different groups ($p < 0.05$). Data are mean \pm SD, $n = 3$ replicates each group.

3.4.4. Western Blot Test

Western blot analysis was used to evaluate the protein expression levels in MC3T3-E1 cells cultured on different samples for 14 days. Figure 12A,B displayed Western blot bands and quantitative analysis, respectively.

Consistent with the gene expression levels, the protein expression levels of ALP, COL1A1 and OCN were all higher in cells incubated with NT-ICA-PLGA, NT-ASP/PLGA and NT-ICA-ASP/PLGA substrates, compared to that on the original Ti and Ti-PLGA surfaces. Especially, NT-ICA-ASP/PLGA substrate revealed enhanced expression levels for all of the osteogenic proteins determined in this experiment than those on the other surfaces, $p < 0.05$. The optimal osteogenesis-related protein expression of the NT-ICA-ASP/PLGA substrate is attributed to the combined effects of both ICA and ASP to facilitate bone formation in osteoblast cells.

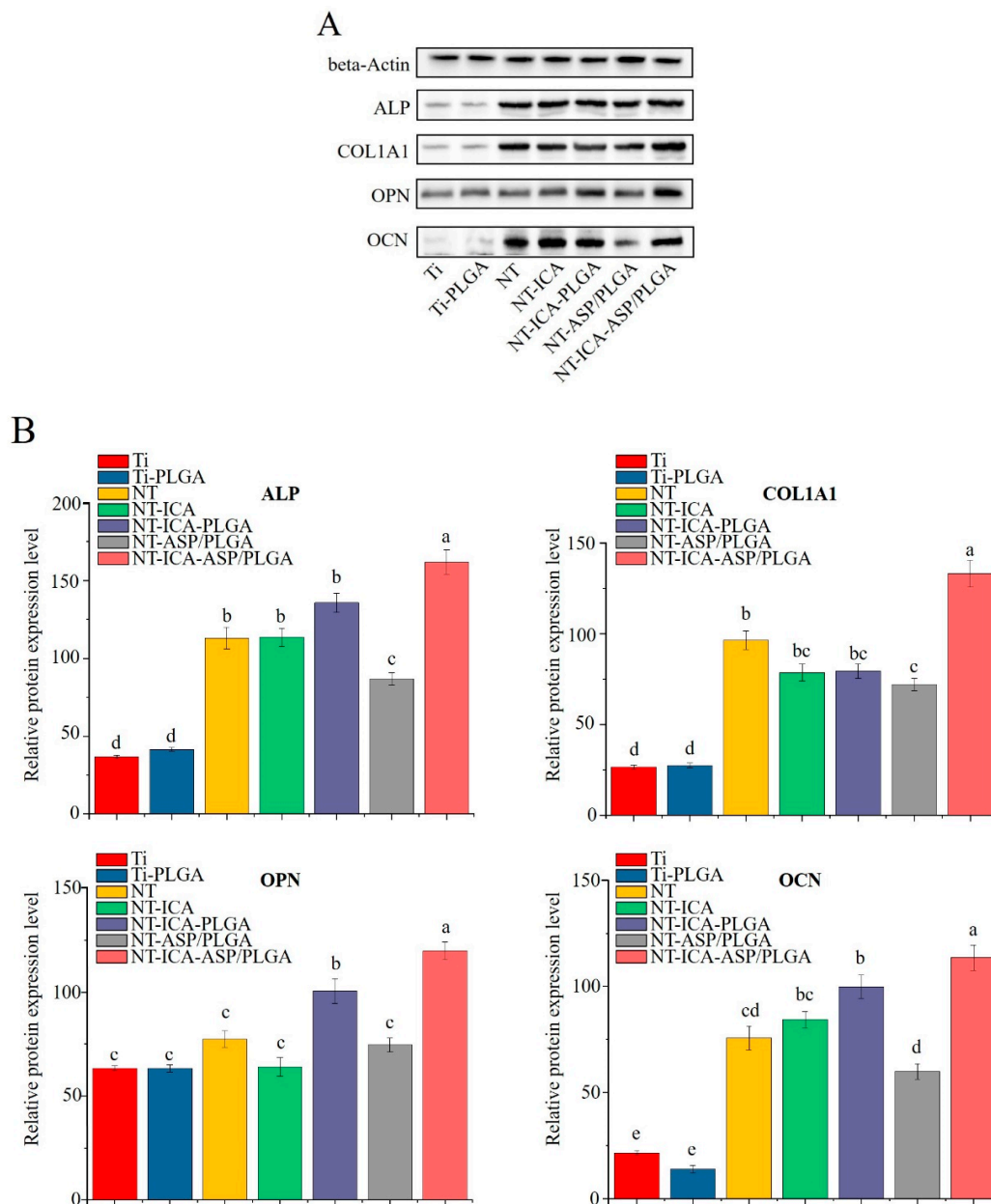


Figure 12. (A) Western blot showing the protein expression levels of ALP, COL1A1, OPN and OCN and beta-Actin in MC3T3-E1 cells after 14 days of culture on different samples. (B) The corresponding gray-scale values of proteins levels in the 7 groups. Different lowercase letters indicate statistically significant differences between different groups ($p < 0.05$). Data are mean \pm SD, $n = 3$ replicates each group.

4. Discussion

Numerous strategies have been implemented to integrate bioactive molecules into the implant surface so as to promote osseointegration. Previously, most investigators endeavored to optimize dental implant materials to promote osteogenic differentiation in mesenchymal stem cells or osteoblast cells and have developed satisfied implant materials to a certain degree. However, only promoting bone formation in osteoblast cells is not enough to fulfill implant osseointegration in vivo. The reason is that after implant were inserted in to the bone tissue, in addition to its interaction with osteoblast, immune cells, such as macrophages, also play an important role in osseointegration [48]. In order to uncover the close relationship between skeletal and immune system, we applied the icariin/aspirin composite

coating on TiO₂ nanotubes surface, named as the NT-ICA-ASP/PLGA substrate, and explore its immunomodulatory effect on macrophage and osteogenic activity in osteoblast cells. We hypothesized that the NT-ICA-ASP/PLGA substrate could induce immunoregulatory function in macrophages and provide an immune microenvironment, which is favorable for osteogenesis in osteoblast cells.

In the current work, the NT-ICA-ASP/PLGA substrate was fabricated. The SEM, XPS detection and contact angle tests confirmed the successful preparation of the icariin/aspirin functionalized coating on TiO₂ nanostructured surface. The established NT-ICA-ASP/PLGA substrate achieved controlled release of both ICA and ASP, with satisfied hydrophilicity. The drug release curves revealed that the releasing period of aspirin is about 7 days, while icariin achieved a sustained release period until 30 days.

To maintain the controlled release of the two kinds of drugs, we firstly prepared TiO₂ nanotubes on the surface of pure titanium by anodization. It is well established that 70–100 nm diameter nanotubes could induce improved cell adhesion, differentiation toward osteoblasts [49–51]. Previously, we have chosen 80 nm diameter nanotubes for the fabrication of functionalized coating [17]. In the present study, we selected a 100 nm diameter of TiO₂ nanotubes for further functionalization study after taking two reasons into considerations. First, as a drug loading reservoir, the larger diameter of the nanotubes, the stronger ability to load drugs [52]; second, 100 nm diameter nanotubes displayed highest ability of protein adsorption, which is critical in mediating cell attachment and proliferation so as to promote bone formation [53,54]. In view of this, we selected 100 nm diameter nanotube as a drug carrier, hoping that it will balance the drug-loading capacity and osteogenic ability at the same time. Another thing should be clarify is that we changed the anodization parameters, compared to our past article [17]. In our previous work, HF was used as an electrolyte, while in the present experiment we employed the reaction system composed of NH₄F, ethylene glycol and water. The reason that we adopted this new method lies in that it can increase the viscosity of the electrolyte and reduce the activity of fluoride ions in order to acquire much controllable and orderly aligned nanotubes with uniform diameter [55]. In present work, we analyzed the bioactivity, gene expression and immune regulatory responses of the established icariin/aspirin composite coating on 100 nm diameter TiO₂ nanotubes. In the future, we will continue to evaluate the influence of different sizes of TiO₂ nanotubes on the biological behaviors of the coated surface.

We further used PLGA to avoid the initial burst release of drug from the TiO₂ nanotubes surface. PLGA is commonly applied in bone tissue engineering because of its favorable mechanical properties and drug-loading capacity [56,57] and used in wound dressings due to its excellent bonding ability [58]. PLGA has also been employed as coating materials on the surface of titanium implants [59,60]. Serving as biodegradable material [61], PLGA polymer-coated nanotube displayed longer drugs release period compared to chitosan-coated nanotubes [62]. In addition, compared with protein growth factor, icariin and aspirin were both chemical stable and heat-resistant drugs [63,64]. More importantly, since we adopted the dip-coating method for preparation of the PLGA coating onto the NT-ICA-ASP/PLGA substrate, this mild coating method could further protect icariin and aspirin from denaturation during the coating procedure and achieve sustained and multiple release of two kinds of drugs at the same time. Therefore, in this way, we successfully superimposed the ASP/PLGA coating onto the ICA loaded TiO₂ nanotubes structure so as to obtain the established NT-ICA-ASP/PLGA substrate. In the future, we will further detect the interfacial adhesion strength between the coating and titanium substrate.

We have previously reported that ICA and TiO₂ nanotubes structures could exert osteogenic effects synergistically [17]. In the present work, apart from its well-established osteogenic effect, we also intend to explore other functions of ICA. Although there is less report about this issue, it has been revealed that icariin could exert anti-inflammatory function [18]. Icariin and its derivate have demonstrated anti-inflammatory effects in macrophage cell lines, human myeloid cells, and a mouse model of inflammation. Additionally the anti-inflammatory effect was concomitant with a down-regulation of IL-10, IL-6 and TNF- α [19]. Other researchers also found that icariin possess significant therapeutic effect on rheumatoid arthritis (RA) clinically [9]. Moreover, the mechanism of

icariin to prevent RA might be related to its immunoregulatory function, which was mediated through the decrease in the cell number of immune cells Th17. Additionally, icariin administration could inhibit IL-17 production [20]. Taking the above-mentioned factors into consideration, we attempt to discover the anti-inflammatory and immunoregulatory functions of ICA in this work. In the present study, during inflammation markers detection, we discovered decreased IL-1 β gene expression and inhibited IL-1 β and TNF- α protein levels on the NT-ICA and NT-ICA-ASP/PLGA surfaces, compared to Ti surface. Moreover, enhanced gene and protein levels of M2 phenotype markers TGF- β and HO-1 were also observed on ICA-loaded surfaces, compared with Ti and Ti-PLGA substrates. These results confirmed the anti-inflammatory and immunoregulatory functions of ICA.

Aspirin (ASP), a classic non-steroidal anti-inflammatory drug, remains the first-line clinical drug due to its good antipyretic and analgesic capabilities and extremely low drug side effects [65]. Some researchers showed that ASP down-regulate iNOS and TNF- α expression in macrophage cells in vitro and improve bone regeneration in vivo by inhibiting LPS-induced macrophage activation in the early stages of inflammation [66]. In addition, aspirin may be a promising option for preventing and curing osteoclastic bone destruction, including peri-implant osteolysis [67]. Another researcher also proved that on the surface of titanium primed with phase-transited lysozyme, a coating loaded with aspirin could promote osseointegration [68]. In our experiment, compared with Ti surface, NT-ASP/PLGA and NT-ICA-ASP/PLGA surfaces displayed decreased IL-1 β gene level and reduced IL-1 β and TNF- α protein levels, with upregulated TGF- β and HO-1 gene and protein expression levels, $p < 0.05$. As expected, our results confirmed the anti-inflammatory and immunoregulatory functions of ASP, with the established NT-ICA-ASP/PLGA substrate exhibiting decreased M1 inflammatory and increased M2 proregenerative effects at the same time.

It is well known that macrophages are the main effector cells of the inflammatory response, and have great plasticity. When stimulated by different signals, they can show a M1 or M2 phenotype [38,39]. The timely transformation of M1-type to M2-type macrophages effectively promotes the regression of inflammation and tissue repair [69,70]. Generally speaking, classically activated macrophages (M1) secrete a variety of proinflammatory factors, such as TNF- α , IL-1 β , IL-6, etc. While the alternatively activated M2 phenotype macrophages generate anti-inflammatory or immunoregulatory cytokines such as TGF- β and IL-10 [71]. In addition, heme oxygenase HO-1, the derivable isoform of the heme-degrading enzyme HO, plays an important role in inflammation and immunoregulation of homeostasis. Myeloid HO-1 expression modulates macrophage polarization to M2 [72,73]. Furthermore, high HO-1 level increased the expression of osteonectin, OPG and BMP-2, and increase osteoblast function and differentiation [74]. In our experiment, down-regulated M1 proinflammatory and up-regulated M2 proregenerative genes and proteins expression were shown on the novel icariin/aspirin composite coating covered TiO₂ nanotubes surface, compared with pure Ti surface. These results indicated that the NT-ICA-ASP/PLGA substrate revealed optimal ability, which could inhibit inflammation and enhance regeneration simultaneously, probably attributed to the synergistic effects of ICA and ASP.

Recently, osteoimmunomodulation (OIM) has been raised to emphasize the importance of immune response during osteogenesis at biomaterial-tissue interface. As the concept of OIM has been gradually accepted, more and more attention has been paid to the positive regulation of immune response at implant-tissue interface so as to accelerate implant osseointegration [75]. After implant insertion, inflammation should be properly regulated to achieve faster bone integration, particularly for patients who are suffering from systemic diseases, which were adverse to bone formation [76,77]. By regulating the early inflammatory response of macrophages, tissue repair can be enhanced, thereby promoting the early rapid formation of bone tissue around the implant.

In order to evaluate OIM, we firstly extracted conditioned media (CM) from macrophage cells incubated with various implant materials. Then the extracted CM was added to osteoblast cells to simulate the immune microenvironment around the implant site. Thus, the indirect coculture system composed of sample slices, macrophage CM and osteoblast cells is ready to evaluate the effects of

immune cells on osteoblast differentiation. Our results suggested that in the coculture system, osteoblast cells on the NT-ASP/PLGA and NT-ICA-ASP/PLGA substrates displayed increased cell proliferation, compared with the other groups at day 5 and 7. Moreover, cells showed well-spread morphology on the NT-ICA-ASP/PLGA substrate, suggesting good cell adhesion on the modified substrate. In addition, we also detected the osteogenic gene and protein levels in the coculture system. During the osteoblast cell differentiation process, an early increase in alkaline phosphatase (ALP) was observed. Then followed by an augment in collagen type 1 and OPN, with osteocalcin expressed later [78]. We measured expression levels of the abovementioned four typical marker genes, including *ALP*, *COL*, *OPN* and *OCN*, which expressed at different stages of osteoblast differentiation and osteogenesis. As predicted, the highest gene levels were observed on the NT-ICA-ASP/PLGA substrate, implying the collaborative pro-osteogenic effect of ICA and ASP at the genetic level. Not only that, both ICA and ASP modified surfaces revealed relatively higher protein levels of osteogenic proteins than pure Ti surface. Especially, the NT-ICA-ASP/PLGA substrate demonstrated the highest expression levels for all of the osteogenesis-related proteins. It is well-accepted that enhanced gene and protein expression levels related to osteoblast cell differentiation may accelerate osseointegration at the implant-tissue interface. The advanced expression levels of both osteogenesis-related genes and proteins on the NT-ICA-ASP/PLGA substrate implied its superior ability to induce osteoblast cells differentiation. The optimal effect of the NT-ICA-ASP/PLGA substrate might be ascribed to the synergistic effects of ICA and ASP, which is in line with its excellent cell proliferation and adhesion results.

5. Conclusions

In view of the concept of OIM, it is especially to be expected to fabricate an implant material, which possesses both early immune regulatory property and long-term osteogenic ability. Both ICA and ASP are candidate drugs for implant surface modification with multiple function including anti-inflammation, immunoregulation and osteogenesis. Taken into consideration of the factors mentioned above, we constructed the NT-ICA-ASP/PLGA substrate. The novel substrate could trigger an effective and timely shift of macrophage from the inflammatory reaction stage to restorative stage. The established NT-ICA-ASP/PLGA surface endowed the modified surface with immunomodulatory function in macrophages and osteogenic effect in osteoblast cells at the same time. This study provides a very promising strategy for fabricating functionalized coating on titanium-based alloys to improve implant osseointegration.

Author Contributions: Conceptualization, Y.L. (Ying Li) and C.L.; Data curation, A.M. and Y.Y.; Funding acquisition, Y.L. (Ying Li) and C.L.; Investigation, A.M., Y.Y., B.C., and W.W.; Methodology, A.M., Y.Y., J.L., H.Q., and Y.L. (Yunkai Liang); Project administration, Y.L. (Ying Li) and C.L.; Writing—original draft, A.M. and Y.Y.; Writing—review and editing, Y.L. (Ying Li). All authors have read and agreed to the published version of the manuscript.

Funding: This research was funded by National Natural Science Foundation of China, Grant No. 81870809, 81500886, 31470920 and Tianjin Natural Science Foundation Grant No. 16JCYBJC28700.

Acknowledgments: We sincerely acknowledge Baoye Li from the School of Materials Science and Engineering, Hebei University of Technology, for her precious technical support and discussions. We also thank Huanhuan Zhai from Tianjin Institute of Industrial Biotechnology, Chinese Academy of Sciences, for her important work in preparing SEM images.

Conflicts of Interest: The authors declare no conflict of interest.

References

1. Elani, H.W.; Starr, J.R.; Da Silva, J.D.; Gallucci, G.O. Trends in Dental Implant Use in the U.S., 1999–2016, and Projections to 2026. *J. Dent. Res.* **2018**, *97*, 1424–1430. [[CrossRef](#)] [[PubMed](#)]
2. Krishna, B.V.; Bose, S.; Bandyopadhyay, A. Low stiffness porous Ti structures for load-bearing implants. *Acta Biomater.* **2007**, *3*, 997–1006. [[CrossRef](#)] [[PubMed](#)]

3. Rani, V.V.; Vinoth-Kumar, L.; Anitha, V.C.; Manzoor, K.; Deepthy, M.; Shantikumar, V.N. Osteointegration of titanium implant is sensitive to specific nanostructure morphology. *Acta Biomater.* **2012**, *8*, 1976–1989. [[CrossRef](#)] [[PubMed](#)]
4. Qing, Y.; Cheng, L.; Li, R.; Liu, G.; Zhang, Y.; Tang, X.; Wang, J.; Liu, H.; Qin, Y. Potential antibacterial mechanism of silver nanoparticles and the optimization of orthopedic implants by advanced modification technologies. *Int. J. Nanomed.* **2018**, *13*, 3311–3327. [[CrossRef](#)] [[PubMed](#)]
5. Yang, B.C.; Zhou, X.D.; Yu, H.Y.; Wu, Y.; Bao, C.Y.; Man, Y.; Cheng, L.; Sun, Y. Advances in titanium dental implant surface modification. *Hua Xi Kou Qiang Yi Xue Za Zhi* **2019**, *37*, 124–129. [[CrossRef](#)]
6. Li, Y.; Song, Y.; Ma, A.; Li, C. Surface Immobilization of TiO₂ Nanotubes with Bone Morphogenetic Protein-2 Synergistically Enhances Initial Preosteoblast Adhesion and Osseointegration. *BioMed Res. Int.* **2019**, *2019*, 5697250. [[CrossRef](#)]
7. Agarwal, R.; Garcia, A.J. Biomaterial strategies for engineering implants for enhanced osseointegration and bone repair. *Adv. Drug Deliv. Rev.* **2015**, *94*, 53–62. [[CrossRef](#)]
8. Lai, M.; Cai, K.; Zhao, L.; Chen, X.; Hou, Y.; Yang, Z. Surface functionalization of TiO₂ nanotubes with bone morphogenetic protein 2 and its synergistic effect on the differentiation of mesenchymal stem cells. *Biomacromolecules* **2011**, *12*, 1097–1105. [[CrossRef](#)]
9. Ren, L.; Pan, S.; Li, H.; Li, Y.; He, L.; Zhang, S.; Che, J.; Niu, Y. Effects of aspirin-loaded graphene oxide coating of a titanium surface on proliferation and osteogenic differentiation of MC3T3-E1 cells. *Sci. Rep.* **2018**, *8*, 15143. [[CrossRef](#)]
10. Thomas, M.V.; Puleo, D.A. Infection, inflammation, and bone regeneration: A paradoxical relationship. *J. Dent. Res.* **2011**, *90*, 1052–1061. [[CrossRef](#)]
11. Zhang, X.; Liu, T.; Huang, Y.; Wismeijer, D.; Liu, Y. Icaritin: Does it have an osteoinductive potential for bone tissue engineering? *Phytother. Res.* **2014**, *28*, 498–509. [[CrossRef](#)] [[PubMed](#)]
12. Song, Y.; Ma, A.; Ning, J.; Zhong, X.; Zhang, Q.; Zhang, X.; Hong, G.; Li, Y.; Sasaki, K.; Li, C. Loading icaritin on titanium surfaces by phase-transited lysozyme priming and layer-by-layer self-assembly of hyaluronic acid/chitosan to improve surface osteogenesis ability. *Int. J. Nanomed.* **2018**, *13*, 6751–6767. [[CrossRef](#)] [[PubMed](#)]
13. Wu, T.; Shu, T.; Kang, L.; Wu, J.; Xing, J.; Lu, Z.; Chen, S.; Lv, J. Icaritin, a novel plant-derived osteoinductive agent, enhances the osteogenic differentiation of human bone marrow- and human adipose tissue-derived mesenchymal stem cells. *Int. J. Mol. Med.* **2017**, *39*, 984–992. [[CrossRef](#)] [[PubMed](#)]
14. Ma, X.N.; Zhou, J.; Ge, B.F.; Zhen, P.; Ma, H.P.; Shi, W.G.; Cheng, K.; Xian, C.J.; Chen, K.M. Icaritin induces osteoblast differentiation and mineralization without dexamethasone in vitro. *Planta Med.* **2013**, *79*, 1501–1508. [[CrossRef](#)]
15. Song, L.; Zhao, J.; Zhang, X.; Li, H.; Zhou, Y. Icaritin induces osteoblast proliferation, differentiation and mineralization through estrogen receptor-mediated ERK and JNK signal activation. *Eur. J. Pharmacol.* **2013**, *714*, 15–22. [[CrossRef](#)]
16. Zhao, J.; Ohba, S.; Komiyama, Y.; Shinkai, M.; Chung, U.I.; Nagamune, T. Icaritin: A potential osteoinductive compound for bone tissue engineering. *Tissue Eng. Part A* **2010**, *16*, 233–243. [[CrossRef](#)]
17. Ma, A.; Shang, H.; Song, Y.; Chen, B.; You, Y.; Han, W.; Zhang, X.; Zhang, W.; Li, Y.; Li, C. Icaritin-Functionalized Coating on TiO₂ Nanotubes Surface to Improve Osteoblast Activity In Vitro and Osteogenesis Ability In Vivo. *Coatings* **2019**, *9*, 327. [[CrossRef](#)]
18. Zhou, J.; Wu, J.; Chen, X.; Fortenbery, N.; Eksioğlu, E.; Kodumudi, K.N.; Pk, E.B.; Dong, J.; Djeu, J.Y.; Wei, S. Icaritin and its derivative, ICT, exert anti-inflammatory, anti-tumor effects, and modulate myeloid derived suppressive cells (MDSCs) functions. *Int. Immunopharmacol.* **2011**, *11*, 890–898. [[CrossRef](#)]
19. Shao, H.; Shen, J.; Wang, M.; Cui, J.; Wang, Y.; Zhu, S.; Zhang, W.; Yang, H.; Xu, Y.; Geng, D. Icaritin protects against titanium particle-induced osteolysis and inflammatory response in a mouse calvarial model. *Biomaterials* **2015**, *60*, 92–99. [[CrossRef](#)]
20. Chi, L.; Gao, W.; Shu, X.; Lu, X. A natural flavonoid glucoside, icaritin, regulates Th17 and alleviates rheumatoid arthritis in a murine model. *Mediat. Inflamm.* **2014**, *2014*, 392062. [[CrossRef](#)]
21. Derry, S.; Moore, R.A. Single dose oral aspirin for acute postoperative pain in adults. *Cochrane Database Syst. Rev.* **2012**, *18*, CD002067. [[CrossRef](#)] [[PubMed](#)]

22. Tang, J.; Xiong, J.; Wu, T.; Tang, Z.; Ding, G.; Zhang, C.; Wang, S.; Liu, Y. Aspirin treatment improved mesenchymal stem cell immunomodulatory properties via the 15d-PGJ2/PPARgamma/TGF-beta1 pathway. *Stem Cells Dev.* **2014**, *23*, 2093–2103. [[CrossRef](#)] [[PubMed](#)]
23. Cao, Y.; Xiong, J.; Mei, S.; Wang, F.; Zhao, Z.; Wang, S.; Liu, Y. Aspirin promotes bone marrow mesenchymal stem cell-based calvarial bone regeneration in mini swine. *Stem Cell Res.* **2015**, *6*, 210. [[CrossRef](#)] [[PubMed](#)]
24. Xie, Y.; Pan, M.; Gao, Y.; Zhang, L.; Ge, W.; Tang, P. Dose-dependent roles of aspirin and other non-steroidal anti-inflammatory drugs in abnormal bone remodeling and skeletal regeneration. *Cell Biosci.* **2019**, *9*, 103. [[CrossRef](#)]
25. Shi, S.; Yamaza, T.; Akiyama, K. Is aspirin treatment an appropriate intervention to osteoporosis? *Future Rheumatol.* **2008**, *3*, 499–502. [[CrossRef](#)]
26. Yamaza, T.; Miura, Y.; Bi, Y.; Liu, Y.; Akiyama, K.; Sonoyama, W.; Patel, V.; Gutkind, S.; Young, M.; Gronthos, S.; et al. Pharmacologic stem cell based intervention as a new approach to osteoporosis treatment in rodents. *PLoS ONE* **2008**, *3*, e2615. [[CrossRef](#)]
27. Wei, S.; Li, Y.; Bai, Y.; Pan, J.; Wang, H.; Li, H.; Xu, X.; Fu, X.; Shi, R.; Luo, Z.; et al. A hybrid 3D-printed aspirin-laden liposome composite scaffold for bone tissue engineering. *J. Mater. Chem. B* **2018**, *7*. [[CrossRef](#)]
28. Maher, S.; Mazinani, A.; Barati, M.R.; Losic, D. Engineered titanium implants for localized drug delivery: Recent advances and perspectives of Titania nanotubes arrays. *Expert Opin. Drug Deliv.* **2018**, *15*, 1021–1037. [[CrossRef](#)]
29. Ahn, T.K.; Lee, D.H.; Kim, T.S.; Jang, G.C.; Choi, S.; Oh, J.B.; Ye, G.; Lee, S. Modification of Titanium Implant and Titanium Dioxide for Bone Tissue Engineering. *Adv. Exp. Med. Biol.* **2018**, *1077*, 355–368. [[CrossRef](#)]
30. Gulati, K.; Ivanovski, S. Dental implants modified with drug releasing titania nanotubes: Therapeutic potential and developmental challenges. *Expert Opin. Drug Deliv.* **2017**, *14*, 1009–1024. [[CrossRef](#)]
31. Rasouli, R.; Barhoum, A.; Uludag, H. A review of nanostructured surfaces and materials for dental implants: Surface coating, patterning and functionalization for improved performance. *Biomater. Sci.* **2018**, *6*, 1312–1338. [[CrossRef](#)] [[PubMed](#)]
32. Wang, Q.; Huang, J.Y.; Li, H.Q.; Chen, Z.; Zhao, A.Z.; Wang, Y.; Zhang, K.Q.; Sun, H.T.; Al-Deyab, S.S.; Lai, Y.K. TiO₂ nanotube platforms for smart drug delivery: A review. *Int. J. Nanomed.* **2016**, *11*, 4819–4834. [[CrossRef](#)]
33. Kapoor, D.N.; Bhatia, A.; Kaur, R.; Sharma, R.; Kaur, G.; Dhawan, S. PLGA: A unique polymer for drug delivery. *Ther. Deliv.* **2015**, *6*, 41–58. [[CrossRef](#)] [[PubMed](#)]
34. Danhier, F.; Ansorena, E.; Silva, J.M.; Coco, R.; Le Breton, A.; Preat, V. PLGA-based nanoparticles: An overview of biomedical applications. *J. Control. Release* **2012**, *161*, 505–522. [[CrossRef](#)] [[PubMed](#)]
35. Pagels, R.F.; Prud'homme, R.K. Polymeric nanoparticles and microparticles for the delivery of peptides, biologics, and soluble therapeutics. *J. Control. Release* **2015**, *219*, 519–535. [[CrossRef](#)] [[PubMed](#)]
36. Wang, J.; Meng, F.; Song, W.; Jin, J.; Ma, Q.; Fei, D.; Fang, L.; Chen, L.; Wang, Q.; Zhang, Y. Nanostructured titanium regulates osseointegration via influencing macrophage polarization in the osteogenic environment. *Int. J. Nanomed.* **2018**, *13*, 4029–4043. [[CrossRef](#)]
37. Zhang, R.; Liu, X.; Xiong, Z.; Huang, Q.; Yang, X.; Yan, H.; Ma, J.; Feng, Q.; Shen, Z. The immunomodulatory effects of Zn-incorporated micro/nanostructured coating in inducing osteogenesis. *Artif. Cells Nanomed. Biotechnol.* **2018**, *46*, 1123–1130. [[CrossRef](#)]
38. Oishi, Y.; Manabe, I. Macrophages in inflammation, repair and regeneration. *Int. Immunol.* **2018**, *30*, 511–528. [[CrossRef](#)]
39. Peiseler, M.; Kubers, P. Macrophages play an essential role in trauma-induced sterile inflammation and tissue repair. *Eur. J. Trauma Emerg. Surg. Off. Publ. Eur. Trauma Soc.* **2018**, *44*, 335–349. [[CrossRef](#)]
40. Minutti, C.M.; Knipper, J.A.; Allen, J.E.; Zaiss, D.M. Tissue-specific contribution of macrophages to wound healing. *Semin. Cell Dev. Biol.* **2017**, *61*, 3–11. [[CrossRef](#)]
41. Korsmeyer, R.W.; Gurny, R.; Doelker, E.; Buri, P.; Peppas, N.A. Mechanisms of solute release from porous hydrophilic polymers. *Int. J. Pharm.* **1983**, *15*, 25–35. [[CrossRef](#)]
42. Sun, X.; Wei, J.; Lyu, J.; Bian, T.; Liu, Z.; Huang, J.; Pi, F.; Li, C.; Zhong, Z. Bone-targeting drug delivery system of biomineral-binding liposomes loaded with icariin enhances the treatment for osteoporosis. *J. Nanobiotechnol.* **2019**, *17*, 10. [[CrossRef](#)] [[PubMed](#)]
43. Lisuzzo, L.; Cavallaro, G.; Parisi, F.; Milioto, S.; Fakhruddin, R.; Lazzara, G. Core/Shell Gel Beads with Embedded Halloysite Nanotubes for Controlled Drug Release. *Coatings* **2019**, *9*, 70. [[CrossRef](#)]
44. Zheng, Y.; Zhu, G.; He, J.; Wang, G.; Li, D.; Zhang, F. Icariin targets Nrf2 signaling to inhibit microglia-mediated neuroinflammation. *Int. Immunopharmacol.* **2019**, *73*, 304–311. [[CrossRef](#)] [[PubMed](#)]

45. El-Shitany, N.A.; Eid, B.G. Icarin modulates carrageenan-induced acute inflammation through HO-1/Nrf2 and NF- κ B signaling pathways. *Biomed. Pharmacother. Biomed. Pharmacother.* **2019**, *120*, 109567. [[CrossRef](#)] [[PubMed](#)]
46. Zhao, L.; Mei, S.; Chu, P.K.; Zhang, Y.; Wu, Z. The influence of hierarchical hybrid micro/nano-textured titanium surface with titania nanotubes on osteoblast functions. *Biomaterials* **2010**, *31*, 5072–5082. [[CrossRef](#)] [[PubMed](#)]
47. Zhao, W.; Li, J.; Jin, K.; Liu, W.; Qiu, X.; Li, C. Fabrication of functional PLGA-based electrospun scaffolds and their applications in biomedical engineering. *Mater. Sci. Eng. C Mater. Biol. Appl.* **2016**, *59*, 1181–1194. [[CrossRef](#)]
48. Chen, Z.; Klein, T.; Murray, R.Z.; Crawford, R.; Chang, J.; Wu, C.; Xiao, Y. Osteoimmunomodulation for the development of advanced bone biomaterials. *Mater. Today* **2016**, *19*, 304–321. [[CrossRef](#)]
49. Cheng, Y.; Yang, H.; Yang, Y.; Huang, J.; Wu, K.; Chen, Z.; Wang, X.; Lin, C.; Lai, Y. Progress in TiO₂ nanotube coatings for biomedical applications: A review. *J. Mater. Chem. B* **2018**, *6*, 1862–1886. [[CrossRef](#)]
50. von Wilmsowsky, C.; Bauer, S.; Roedl, S.; Neukam, F.W.; Schmuki, P.; Schlegel, K.A. The diameter of anodic TiO₂ nanotubes affects bone formation and correlates with the bone morphogenetic protein-2 expression in vivo. *Clin. Oral Implant. Res.* **2012**, *23*, 359–366. [[CrossRef](#)]
51. Yu, W.-Q.; Jiang, X.-Q.; Zhang, F.-Q.; Xu, L. The effect of anatase TiO₂ nanotube layers on MC3T3-E1 preosteoblast adhesion, proliferation, and differentiation. *J. Biomed. Mater. Res. A* **2010**, *94A*, 1012–1022. [[CrossRef](#)] [[PubMed](#)]
52. Torres, C.C.; Campos, C.H.; Díaz, C.; Jiménez, V.A.; Vidal, F.; Guzmán, L.; Alderete, J.B. PAMAM-grafted TiO₂ nanotubes as novel versatile materials for drug delivery applications. *Mater. Sci. Eng. C Mater. Biol. Appl.* **2016**, *65*, 164–171. [[CrossRef](#)] [[PubMed](#)]
53. Yang, W.; Xi, X.; Ran, Q.; Liu, P.; Hu, Y.; Cai, K. Influence of the titania nanotubes dimensions on adsorption of collagen: An experimental and computational study. *Mater. Sci. Eng. C Mater. Biol. Appl.* **2014**, *34*, 410–416. [[CrossRef](#)] [[PubMed](#)]
54. Kulkarni, M.; Mazare, A.; Park, J.; Gongadze, E.; Killian, M.S.; Kralj, S.; von der Mark, K.; Igljic, A.; Schmuki, P. Protein interactions with layers of TiO₂ nanotube and nanopore arrays: Morphology and surface charge influence. *Acta Biomater.* **2016**, *45*, 357–366. [[CrossRef](#)] [[PubMed](#)]
55. Ya, J.; An, L.; Liu, Z.; E, L.; Zhao, W.; Zhao, D.; Liu, C. Investigation of surface morphologies of TiO₂ nanotube arrays by anodization in ethylene glycol electrolytes. *J. Optoelectron. Adv. Mater.* **2011**, *13*, 684–688.
56. Bao, H.; Lv, F.; Liu, T. A pro-angiogenic degradable Mg-poly(lactic-co-glycolic acid) implant combined with rhbFGF in a rat limb ischemia model. *Acta Biomater.* **2017**, *64*, 279–289. [[CrossRef](#)] [[PubMed](#)]
57. Mehrasa, M.; Asadollahi, M.A.; Ghaedi, K.; Salehi, H.; Arpanaei, A. Electrospun aligned PLGA and PLGA/gelatin nanofibers embedded with silica nanoparticles for tissue engineering. *Int. J. Biol. Macromol.* **2015**, *79*, 687–695. [[CrossRef](#)]
58. Daristotle, J.L.; Lau, L.W.; Erdi, M.; Hunter, J.; Djoum, A., Jr.; Srinivasan, P.; Wu, X.; Basu, M.; Ayyub, O.B.; Sandler, A.D.; et al. Sprayable and biodegradable, intrinsically adhesive wound dressing with antimicrobial properties. *Bioeng. Transl. Med.* **2020**, *5*, e10149. [[CrossRef](#)]
59. Yang, Y.; Ren, S.; Zhang, X.; Yu, Y.; Liu, C.; Yang, J.; Miao, L. Safety and efficacy of PLGA(Ag-Fe₃O₄)-coated dental implants in inhibiting bacteria adherence and osteogenic inducement under a magnetic field. *Int. J. Nanomed.* **2018**, *13*, 3751–3762. [[CrossRef](#)]
60. Kazek-Kesik, A.; Nosol, A.; Plonka, J.; Smiga-Matuszowicz, M.; Golda-Cepa, M.; Krok-Borkowicz, M.; Brzychczy-Wloch, M.; Pamula, E.; Simka, W. PLGA-amoxicillin-loaded layer formed on anodized Ti alloy as a hybrid material for dental implant applications. *Mater. Sci. Eng. C Mater. Biol. Appl.* **2019**, *94*, 998–1008. [[CrossRef](#)]
61. Kumari, A.; Yadav, S.K.; Yadav, S.C. Biodegradable polymeric nanoparticles based drug delivery systems. *Colloids Surf. B-Biointerfaces* **2010**, *75*, 1–18. [[CrossRef](#)] [[PubMed](#)]
62. Gulati, K.; Ramakrishnan, S.; Aw, M.S.; Atkins, G.J.; Findlay, D.M.; Losic, D. Biocompatible polymer coating of titania nanotube arrays for improved drug elution and osteoblast adhesion. *Acta Biomater.* **2012**, *8*, 449–456. [[CrossRef](#)] [[PubMed](#)]
63. Wu, T.; Nan, K.; Chen, J.; Jin, D.; Jiang, S.; Zhao, P.; Xu, J.; Du, H.; Zhang, X.; Li, J.; et al. A new bone repair scaffold combined with chitosan/hydroxyapatite and sustained releasing icariin. *Chin. Sci. Bull.* **2009**, *54*, 2953–2961. [[CrossRef](#)]

64. Banerjee, P.K.; Amidon, G.L. Physicochemical property modification strategies based on enzyme substrate specificities I: Rationale, synthesis, and pharmaceutical properties of aspirin derivatives. *J. Pharm. Sci.* **1981**, *70*, 1299–1303. [[CrossRef](#)] [[PubMed](#)]
65. Vane, J.R.; Botting, R.M. The mechanism of action of aspirin. *Thromb Res.* **2003**, *110*, 255–258. [[CrossRef](#)]
66. Liu, Y.; Fang, S.; Li, X.; Feng, J.; Du, J.; Guo, L.; Su, Y.; Zhou, J.; Ding, G.; Bai, Y.; et al. Aspirin inhibits LPS-induced macrophage activation via the NF-kappaB pathway. *Sci. Rep.* **2017**, *7*, 11549. [[CrossRef](#)]
67. Shi, J.; Wang, Z.; Guo, X.; Shen, J.; Sun, H.; Bai, J.; Yu, B.; Wang, L.; Zhou, W.; Liu, Y.; et al. Aspirin inhibits osteoclast formation and wear-debris-induced bone destruction by suppressing mitogen-activated protein kinases. *J. Cell. Physiol.* **2020**, *235*, 2599–2608. [[CrossRef](#)]
68. Zhang, W.; Lu, X.; Yuan, Z.; Shen, M.; Song, Y.; Liu, H.; Deng, J.; Zhong, X.; Zhang, X. Establishing an osteoimmunomodulatory coating loaded with aspirin on the surface of titanium primed with phase-transited lysozyme. *Int. J. Nanomed.* **2019**, *14*, 977–991. [[CrossRef](#)]
69. Brown, B.N.; Ratner, B.D.; Goodman, S.B.; Amar, S.; Badylak, S.F. Macrophage polarization: An opportunity for improved outcomes in biomaterials and regenerative medicine. *Biomaterials* **2012**, *33*, 3792–3802. [[CrossRef](#)]
70. Miron, R.J.; Bosshardt, D.D. OsteoMacs: Key players around bone biomaterials. *Biomaterials* **2016**, *82*, 1–19. [[CrossRef](#)]
71. Shapouri-Moghaddam, A.; Mohammadian, S.; Vazini, H.; Taghadosi, M.; Esmaili, S.A.; Mardani, F.; Seifi, B.; Mohammadi, A.; Afshari, J.T.; Sahebkar, A. Macrophage plasticity, polarization, and function in health and disease. *J. Cell. Physiol.* **2018**, *233*, 6425–6440. [[CrossRef](#)] [[PubMed](#)]
72. Vijayan, V.; Wagener, F.; Immenschuh, S. The macrophage heme-heme oxygenase-1 system and its role in inflammation. *Biochem. Pharm.* **2018**, *153*, 159–167. [[CrossRef](#)] [[PubMed](#)]
73. Zhang, M.; Nakamura, K.; Kageyama, S.; Lawal, A.O.; Gong, K.W.; Bhetraratana, M.; Fujii, T.; Sulaiman, D.; Hirao, H.; Bolisetty, S.; et al. Myeloid HO-1 modulates macrophage polarization and protects against ischemia-reperfusion injury. *JCI Insight* **2018**, *3*. [[CrossRef](#)] [[PubMed](#)]
74. Barbagallo, I.; Vanella, A.; Peterson, S.J.; Kim, D.H.; Tibullo, D.; Giallongo, C.; Vanella, L.; Parrinello, N.; Palumbo, G.A.; Di Raimondo, F.; et al. Overexpression of heme oxygenase-1 increases human osteoblast stem cell differentiation. *J. Bone Min. Metab.* **2010**, *28*, 276–288. [[CrossRef](#)] [[PubMed](#)]
75. Hotchkiss, K.M.; Reddy, G.B.; Hyzy, S.L.; Schwartz, Z.; Boyan, B.D.; Olivares-Navarrete, R. Titanium surface characteristics, including topography and wettability, alter macrophage activation. *Acta Biomater.* **2016**, *31*, 425–434. [[CrossRef](#)]
76. Aghaloo, T.; Pi-Anfruns, J.; Moshaverinia, A.; Sim, D.; Grogan, T.; Hadaya, D. The Effects of Systemic Diseases and Medications on Implant Osseointegration: A Systematic Review. *Int. J. Oral Maxillofac. Implant.* **2019**, *34*, s35–s49. [[CrossRef](#)]
77. Smeets, R.; Henningsen, A.; Jung, O.; Heiland, M.; Hammacher, C.; Stein, J.M. Definition, etiology, prevention and treatment of peri-implantitis-a review. *Head Face Med.* **2014**, *10*, 34. [[CrossRef](#)]
78. Eleniste, P.P.; Patel, V.; Posritong, S.; Zero, O.; Largura, H.; Cheng, Y.H.; Himes, E.R.; Hamilton, M.; Baughman, J.; Kacena, M.A.; et al. Pyk2 and Megakaryocytes Regulate Osteoblast Differentiation and Migration Via Distinct and Overlapping Mechanisms. *J. Cell Biochem.* **2016**, *117*, 1396–1406. [[CrossRef](#)]

